INSTITUTE

FOR

AEROSPACE STUDIES

UNIVERSITY OF TORONTO

GEOSTATIONARY ORBITAL ESTIMATION

USING A KALMAN FILTER

G. B. Sincarsin

Report to
Department of Communications
DSS Contract No. O3SU. 36100-1-0154 OSU81-00092

November, 1982.

checked 10/83

(2)

GEOSTATIONARY ORBITAL ESTIMATION

USING A KALMAN FILTER

(1)
G. B. Sincarsin

November, 1982

DD 4493507
DL 4493553

Acknowledgements

The author is pleased to acknowledge the assistance of the following persons. Thanks are due

Units and Spelling

This report uses SI units and North American spelling.

Summary

The ability of a 'sequential' Kalman filter to predict a geostationary and an approximately geostationary orbit is assessed by comparison with the corresponding orbits predicted by a least-squares 'batch' estimator. Prior to performing this comparison, the perturbation models and observations assumed in each estimator are compared and shown to be essentially the same (except for atmospheric drag). An analytical expression for the state noise matrix, assuming a geostationary reference orbit, is given and used during numerical studies. Numerical results indicate that the Kalman Filter performs well for the case of a geostationary orbit (in the absence of orbital perturbations the true state is that of an ideally geostationary orbit). For an approximately geostationary orbit (in the absence of orbital perturbations the true state is only approximately that of a geostationary orbit) the performance of the Kalman filter degrades to the point of 'neutral' stability. A parameter study, in which the values of the initial error covariance matrix, the measurement noise matrix and the state noise matrix are individually varied, is conducted to assess the sensitivity of the Kalman filter's performance. It is observed that the nominal values assigned to each of the above matrices are very near their optimums. It is concluded, therefore, that to improve the Kalman Filter's performance it is the analytical forms assumed for the error and noise matrices (in particular, the state noise matrix for the present study), and not the values normally assigned to these matrices, that deserves further study.

Table of Contents

List of Figures

List of Tables

1. INTRODUCTION

It is the purpose of this study to compare the performance of the Orbit Determination Prediction and Correction (ODPAC) Kalman filter estimator with that of the Goddard Trajectory Determination System (GTDS) Least-Squares estimator, in the application of estimating the orbit of a geostationary satellite when only range measurements are available. An attempt will be made to determine and correct the factors which contribute to the relatively poor performance of the Kalman estimator.

The use of a Kalman filter in orbital estimation is a well-established practice [Brogan and Lemay, 1973]. Furthermore, the application of sequential filtering to the problem of estimating a geostationary orbit is also a well developed field of study (see, for example [Soop, 1980]). The present complication is that only range observations are to be permitted. The literature in this area is somewhat limited. As a major literature search is beyond the scope of this work, much of what follows makes use of the pioneering work by [Brogan and Lemay, 1968] in the area of orbit determination at geostationary altitude. In particular, the possibility of implementing a state noise matrix, obtained by assuming a geostationary reference orbit for the linearizations implicit in the formulation of the extended Kalman filter, is studied. A recent publication [Wakker and Ambrosius, 1982], dedicated to orbit estimation using only laser ranging measurements, cites the importance to numerical performance of predicting the state transition matrix and the state noise matrix. As will be shown, the choice of a geostationary reference orbit also has implications for the resultant form of the state transition matrix.

Prior to undertaking this task, however, a comparison of the ODPAC and GTDS perturbation models will be undertaken to identify and remove any

1

sources of discrepancy which could bias the numerical comparison of the performance of the two routines. Also, simulated and actual range measurements will be compared in an effort to establish whether or not the use of simulated rather than actual range measurements is valid for comparison purposes. The use of the former would greatly facilitate the research process, while still permitting the option of using actual range measurements in a final verification run. The theoretical implications of the present study are then discussed within the context of the governing equations and the mathematical assumptions implicit in ODPAC ([Chodas, 1981] and [Browne and McPherson, 1978]). Finally, a numerical assessment of the ability of the ODPAC Kalman estimator to determine the orbit of a geostationary and an approximately geostationary satellite is conducted. To guarantee valid comparisons, the parameters and initial estimated state used by GTDS to determine the true orbit are assumed.

2. COMPARISON OF PERTURBATION MODELS

Five sources of orbital perturbations are modeled in ODPAC. By appropriately setting a flag or defining a scalar to be nonzero, one can choose to include the effects of Earth's aspherical gravitational field, atmospheric drag, solar gravity, lunar gravity and solar radiation pressure on the orbital motion of a satellite. It is also possible to include a correction for the precession and nutation of Earth's polar axis caused by solar and lunar gravity. This permits a more accurate representation of the satellite's orbit in inertial coordinates.

As ODPAC can both simulate and estimate a satellite's orbit, the same perturbation models are available to both the simulation and estimation

2

software. However, the simulator and estimator need not include the same perturbation sources simultaneously. When solar and lunar gravitational effects on the satellite and Earth are included in both, the constants assumed in the perturbation models are identical. It is possible, however, to select different drag and solar radiation pressure coefficients for use in the simulator and estimator. Also, while the numerical values for the gravitational harmonics caused by the Earth's oblateness are the same regardless of whether they are modeled in the simulator or the estimator, the number of harmonics included in each need not be the same.

In what follows, the perturbation models used in ODPAC will be compared with their GTDS counterparts. The intent is to isolate and remove any differences prior to performing a numerical comparison of the estimated orbital state vectors obtained from each routine.

2.1 Earth's Aspherical Gravitational Field

The model for the gravitational potential of the Earth assumed in ODPAC is given in [Browne and McPherson, 1978 (pp. 3-7, 3-11)], while that assumed in GTDS can be found in [Cappellari, Velez and Fuchs, 1976 (pp. 4-9, 4-22)]. (Henceforth, page references for the above two documents will be made without citing the reference directly.) Except for minor notational differences the governing equations are identical. Furthermore, the harmonic coefficients (J_n - zonal; S_n^m, C_n^m - sectorial when m = n and tesseral when m < n) assumed in each model are numerically identical to seven significant digits for $m \leq n = (1, 2, 3, 4)$. While higher harmonics are permitted in the GTDS software ODPAC is limited to the harmonics cited above, the values of which can be found in [McPherson and Copeck, 1980]. It is necessary, therefore, to restrict numerical comparison of GTDS and ODPAC results to those in which

3

$n \leq 4$. GTDS also includes 'indirect oblation' effects absent in ODPAC; however, these are of secondary importance for the present study.

2.2 Atmospheric Drag

The ODPAC (pp. 3-12, 3-16) and GTDS (pp. 4-22, 4-60) atmospheric drag models use the same defining relation to compute the deceleration of a spherical satellite moving through the atmosphere. However, ODPAC uses a simpler model for the atmosphere than that adopted in GTDS. (GTDS offers two different atmospheric density models, the Modified Harris-Priester model and an analytical formulation of the Jacchia 1971 model.) This difference in atmospheric modeling implies that direct numerical comparison of the states generated by ODPAC and GTDS, when atmospheric drag is present, will reflect differences not only from the estimation technique employed but also from the different atmospheric density profiles assumed in each program. Happily, for geostationary satellites, atmospheric drag can be neglected, thus avoiding this problem for the present study.

It is noteworthy that GTDS also has the capability to treat the drag coefficient and errors in the atmospheric density as extra state variables, to which differential correction can be applied. Furthermore, GTDS can consider cylindrical satellites (with or without solar panels oriented at arbitrary angles to the axis of the cylinder) in drag calculations.

2.3 Solar and Lunar Gravity

The gravitational attractions of the sun and the moon (assumed to be point masses) and the subsequent accelerations experienced by the satellite are modeled identically (again, except for minor notational differences) in ODPAC (pp. 3-17) and GTDS (pp. 4-4, 4-8). Furthermore, the gravitational

4

constants assumed for the sun and the moon are the same in both routines
(see Table 1).

<div align="center">

Table 1

Comparison of Constants

</div>

Constant	Variable	ODPAC Value	GTDS Value
Gravitational Constant (km^3/sec^2)			
– Earth	μ	3.9860080^{15}*	3.9860080^{15}
– Sun	μ_s	1.3271545^{11}	1.3271545^{11}
– Moon	μ_m	4.902778^{3}	4.902778^{3}
Astronomical Unit (km)	AU	1.496^{8}	1.4959789^{8}
Solar Constant (N/m^2)	p	4.5^{-6}	4.5^{-6}
Earth			
– Semi-Major Axis (km)	a_e	6.37814^{3}	6.37814^{3}
– Angular Velocity (deg/sec)	ω_e	4.178074623^{-3}	4.170746^{-3}

*$A^{15} = A \times 10^{15}$.

2.4 Solar Radiation Pressure

The form of the solar radiation perturbation model adopted in both
ODPAC (pp. 3-18) and GTDS (pp. 4-60, 4-65) is

$$\vec{a} = \nu \; K \; P \left(\frac{a_s}{r_s} \right)^2 \hat{\vec{r}}_s \qquad (2.1)$$

where $\vec{a}$ is the acceleration of the spacecraft caused by solar pressure,
ν is the eclipse factor ($\nu = 0$ if the spacecraft is in an eclipse region,
$\nu = 1$ otherwise), K is the solar radiation pressure coefficient, P is the

solar constant (4.5×10^{-6}N/m^2), a_s is the mean Earth-sun distance (1 AU) and $\hat{\vec{r}}_s$ ($= \vec{r}_s/r_s$) is a unit vector in the direction of the incident radiation. In ODPAC $\hat{\vec{r}}_s$ is assumed to be the vector from the sun to the Earth, while in GTDS $\hat{\vec{r}}_s$ is taken to be the vector from the sun to the spacecraft. Hence, in ODPAC parallax is neglected. Also, the numerical value assigned to 1 AU is slightly different in the two routines (see Table 1). Furthermore, the definition of what constitutes eclipse is different in each program. GTDS assumes a cylindrical shadow model, with $\nu = 0$ whenever the spacecraft is within this shadow. ODPAC assumes a more complicated shadow model (containing both penumbral and umbral eclipse regions), with $\nu = 0$ whenever the light intensity is $\leq 50\%$.

The solar radiation pressure coefficient K obeys the relation

$$K = C_r(A/m) \qquad\qquad (2.2)$$

where C_r is the coefficient of reflectivity ($0 \leq C_r \leq 2$), A is the exposed area of the spacecraft and m is the spacecraft's mass. In ODPAC, K must be specified, while in GTDS, given A and m, C_r can be treated as an extra state variable, to which differential correction can be applied.

2.5 Precession and Nutation of Earth's Polar Axis

To define the true equator relative to inertial space one must correct for the precession and nutation of the Earth's polar axis. Correction for precession alone yields the mean equator relative to inertial space, while a subsequent correction for nutation produces the true equator. ODPAC and GTDS use identical transformations from the mean equator and mean equinox to the true equator and true equinox reference frames. The precession of

the ecliptic plane relative to inertial space is neglected in ODPAC but corrected for in GTDS. Furthermore, ODPAC neglects the fact that the polar axis (the normal to the true equator) does not exactly coincide with the spin axis of the Earth. This affects the transformation from the true equator and true equinox frame to the Earth-fixed reference frame. As noted in [Browne and McPherson, 1978], the first effect corresponds to less than 50 arc seconds per century, while the second effect is less than 2 arc seconds. (The spin axis in fact 'wanders' over a distance of approximately 30m at the Earth's surface.)

2.6 Evaluation of the Differences in the Perturbation Models

As highlighted in the previous sections, the perturbation models adopted in ODPAC, for the most part, are very similar to those used in GTDS. For the purposes of the present study, atmospheric drag can be neglected, hence the perturbation model which is most dissimilar is not of concern here. To assess the importance of the other differences an ephemeris run was conducted using ODPAC and compared to an existing GTDS ephemeris run for the Communications Technology Satellite (A = 1.9797×10^{-5}/km^2, m = 332.8 kg). Assuming the same initial state as that used in the GTDS run, and including the following sources of orbital perturbations,

(1) Gravitational Harmonics (n $\leq$ 4, all m $\leq$ 4)

(2) No Atmospheric Drag

(3) Solar Gravity

(4) Lunar Gravity

(5) Solar Radiation Pressure (K = 4.7736107×10^{-8} km^2/kg

     – based on GTDS data)

the position and velocity errors obtained using ODPAC are as shown in Fig. 1

POSITION ERROR (km)

Epoch :   July 4, 1979   12 hr   0 min   0 sec
Final Date :   July 7, 1979   12 hr   0 min   0 sec
Duration :   3 Days   12 hr   0 min   0 sec

Initial $|\underrightarrow{R}|$: 42211.41667 km

TIME (hr)

VELOCITY ERROR (km/sec)

Initial $|\underrightarrow{V}|$: 3.072162075 km/sec
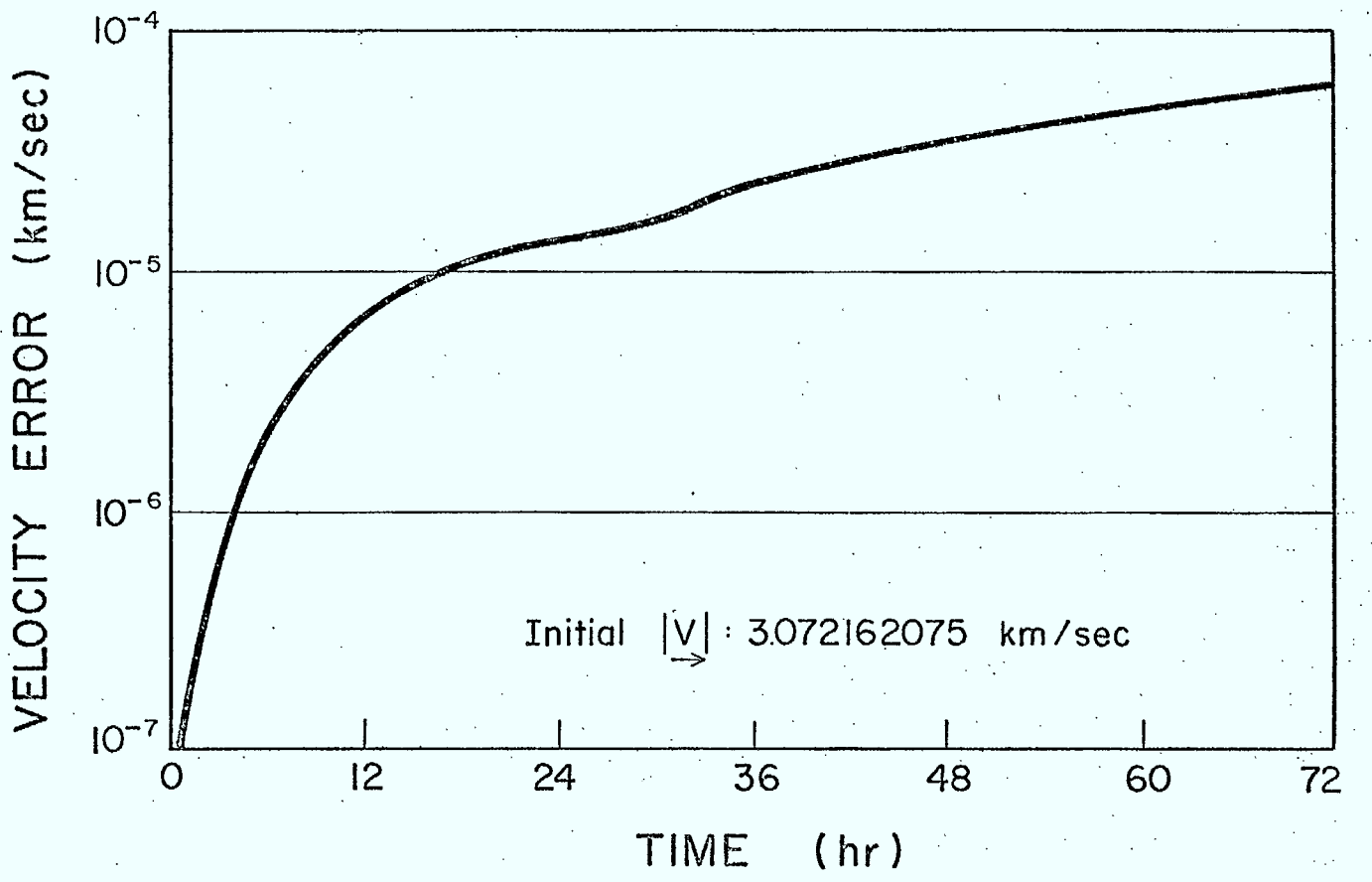
TIME (hr)
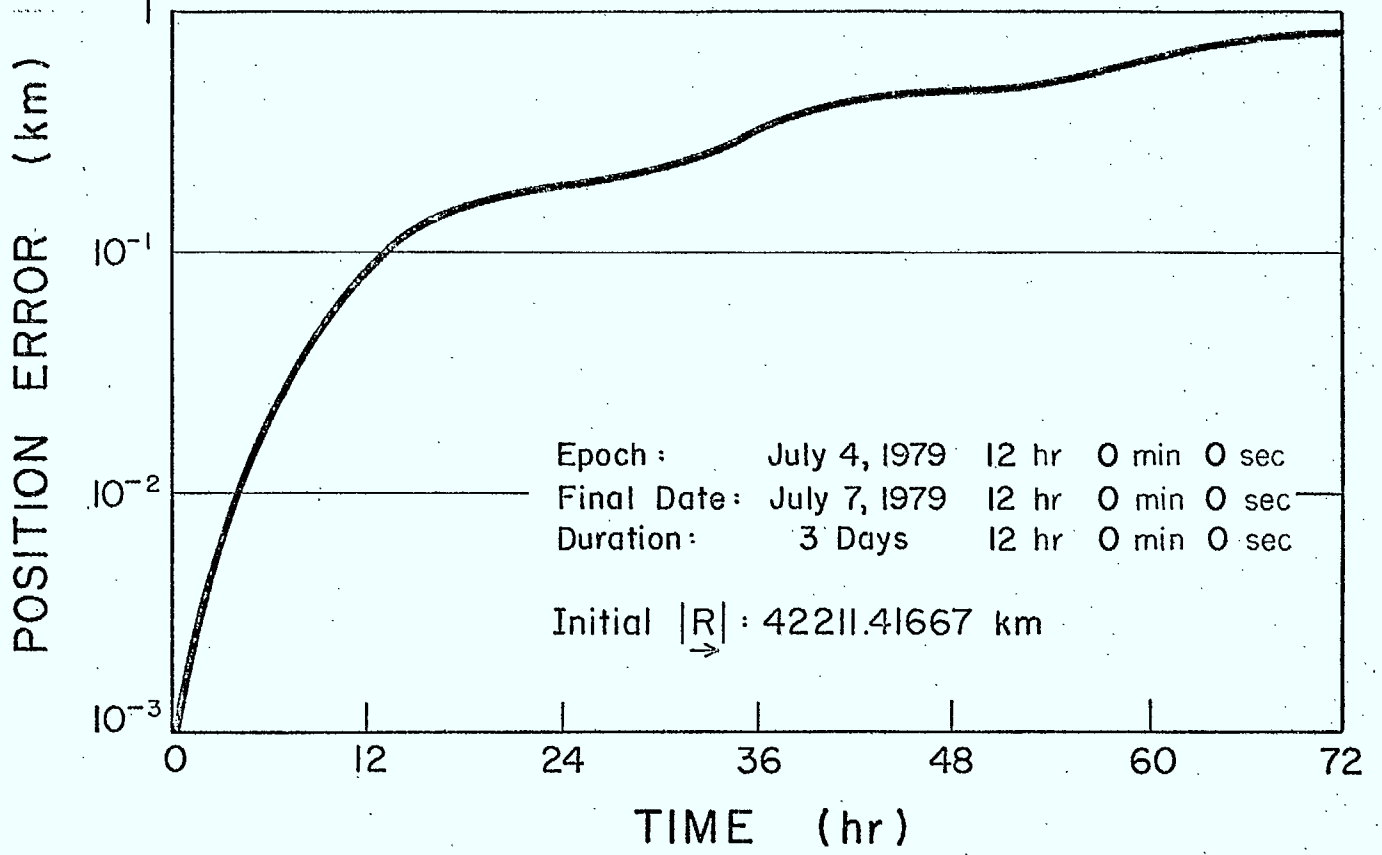
FIGURE 1.   ODPAC SIMULATOR ERRORS.

8

(i.e., the GTDS run was assumed to be correct). A correction was also
applied during the ephemeris run to account for the precession and nutation
of the Earth's polar axis.

Both the position and velocity errors initially increase rapidly; however,
near the end of the run these errors change more slowly. The position error
remains less than 1 km, or 2.4×10^{-3}% of the initial orbital radius, while
the velocity error remains less than 10^{-4} km/sec, or 3.3×10^{-3}% of the initial
velocity. These errors may appear small; however, they must be considered
within the context of this study. The intent is to ascertain why a Kalman
estimator (ODPAC) performs poorly relative to a least-squares estimator
(GTDS) when the orbit of a geostationary satellite is being predicted. The
least-squares estimator begins with an a priori estimate (at epoch) and
applies differential correction using observations in a 'batch' mode to
obtain the true state at epoch. The orbit can then be predicted forward
to some desired time. A Kalman estimator begins with an estimated state
(the least-square a priori estimate) and an error covariance matrix (based
on the difference between the a priori estimated state and the true state
at epoch — here obtained directly from GTDS data). This estimator then
proceeds forward in time processing observations in a sequential mode. To
compare the two estimators it is necessary to choose some time $t_1 > t_0$
(time at epoch) and obtain the state as predicted forward in time using the
true state at epoch from the least-squares estimator. This then becomes
the true state to which the Kalman estimator must converge over the period
$(t_1 - t_0)$. Therefore, ideally, the simulated true state to which the Kalman
estimator is attempting to converge is that given by the GTDS ephemeric run
(t_1 is just some time during this run). Unfortunately, ODPAC does not have
a facility for reading the simulated true state from an external file,

9

hence it must produce its own simulated 'true state' trajectory. Figure 1 suggests that the longer one simulates the orbit using ODPAC the poorer its simulated true state becomes in comparison with the GTDS simulated true state. That is, direct numerical comparison is not truly possible. In fact, after approximately three days the ODPAC-simulated true state deviates from that given by GTDS by the same order of magnitude as the a priori estimated and true state at epoch. Consequently, the best that can be achieved without drastically modifying ODPAC is to accept its simulated orbit as the 'true state' trajectory. One commences the simulation with the true state at epoch determined using GTDS, and sets the estimated state equal to the a priori estimate from GTDS. One then tries to minimize the difference between the estimated and true state. Provided this process yields an acceptable minimum, it can be argued that had the 'true' true state trajectory been available the Kalman estimator would reproduce the GTDS results. Of course, there still remains the issue of real versus simulated observations. This is the subject of the next chapter.

One final comment with regard to Fig. 1 is appropriate. ODPAC and GTDS use different numerical integration schemes. ODPAC performs Cowell's method using a fourth-order Runge-Kutta integrator, while GTDS performs the same method using a twelfth-order Adams predictor (partially corrected) integrator. Thus some of the position and velocity errors in Fig. 1 may be caused by differences in these numerical integration schemes rather than by differences in the perturbation models. GTDS does offer other integration methods and numerical integrators; however, they are not more similar to those used in ODPAC than the combination cited above. Again, to achieve a completely consistent numerical comparison, either ODPAC or GTDS would have to be modified.

3. COMPARISON OF OBSERVATIONS

In an attempt to keep the numerical comparison between ODPAC and GTDS as meaningful as possible it is desirable to replicate the observations used by GTDS in ODPAC. To ensure this the same site locations must be used. Furthermore, not only must the type of observations and their numerical values be the same, but the scheduling and frequency of the observations must be reproduced. The numerical values for the observations can be either numerically simulated by ODPAC or supplied directly in the form of real observations through an external disk file. The first method is more conducive to a research effort where isolating the causes for differences between the numerical performance of ODPAC and GTDS is the goal, as is the case here. It permits a greater degree of flexibility, unlike the second method which, apart from supplying more realism, restricts the number of parameters which can be varied. Also, initially simulating the observations does not preclude confirming the Kalman estimator's performance later with real observations. For these reasons the first alternative is chosen; however, in what follows a comparison of the simulated and real observations is also supplied to confirm the acceptability of the observations used in this study.

3.1 Chosen Case Study

In the previous chapter the results from a GTDS ephemeris run for the Communications Technology Satellite were compared with those from what was essentially an equivalent ODPAC ephemeris run. Here, we use the GTDS least-squares estimation run which provided the initial true state for the ephemeris runs as the case chosen for study: reference number DC/OUT790705, 292357A dated July 5, 1979, 17:14 hrs. In fact, the GTDS ephemeris run is appended

11

to the end of the GTDS estimation run. The site and observation data which follow are all taken from, or related to, this particular run.

3.2 Site Locations

Two site locations are given in the GTDS estimation run; however, only the Ottawa site makes any observations. The locations of both sites are given in Table 2. It should be noted that the adopted reference ellipsoid is that assumed in the GTDS run and not the default ellipsoid given in ODPAC.

Table 2

Site Locations

Name	Ottawa (OTT)	Building 46 (BG46)
Geodetic Latitude (deg. North)	45.347206944	45.352763889
East Longitude (deg.)	284.10969806	284.09733611
Height Above Reference Ellipsoid (km)	0.0834506	0.082
Horizon Elevation (deg.)	0.0	0.0
Reference Ellipsoid – Semi-Major Axis (km) – Eccentricity	6378.166 0.081813333	6378.166 0.081813333

3.3 Observation Summary

The allowable observations in ODPAC are azimuth, elevation, range and range rate. For the present study only range observations are considered. A summary of the important time events governing the observations and the frequency of the observations, as inferred from the GTDS estimation run, is provided in Table 3. To aid in visualizing the positions of the

12

various observation spans (periods in which observations are taken) within the time frame of the GTDS run, a line chart has been included in Fig. 2. Table 4 contains a list of the 96 observations taken during the first and second observation spans.

Table 3

Observation Summary

Epoch:	July 4, 1979
Observations Start:	July 4, 1979
Observations End:	July 5, 1979

Observation Span No.	Commence* Observations	Halt Observations	Duration	Number of Observations	Observation Interval
1	5180				
		5650	470	48	10
2	8900				
		9370	470	48	10
3	14470				
		14940	470	48	10
4	21610				
		22080	470	48	10
5	28810				
		29280	470	48	10
6	36010				
		36480	470	48	10
7	43810				
		44280	470	48	10
8	51790				
		52260	470	48	10
9	57600				
		58070	470	48	10
10	65410				
		65880	470	48	10
11	71970				
		72440	470	48	10
12	77020				
		77250	230	24	10
13	77300				
		77770	470	48	10
14	82820				
		83290	470	48	10

*Time from Epoch in seconds.

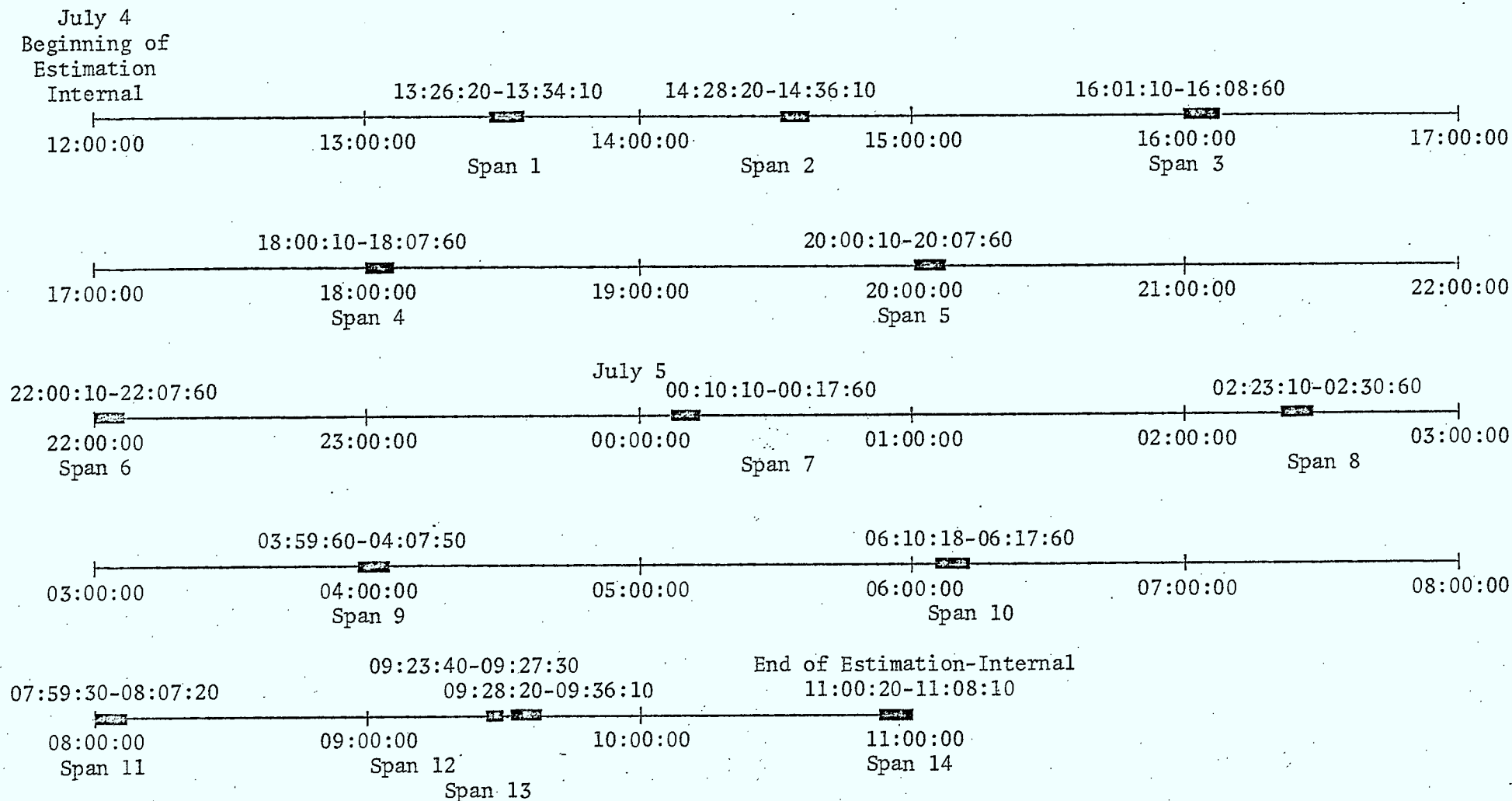FIGURE 2. LOCATIONS OF OBSERVATION SPANS WITHIN GTDS ESTIMATION RUN.

Table 4

Comparison of Actual and Simulated Observations

	Span 1			Span 2	
Observation Number	Actual Range (+ 39269 km)	Simulated Range	Observation Number	Actual Range (+ 39255 km)	Simulated Range
1	0.5752	0.6291	1	1.3034	1.3516
2	0.5512	0.5941	2	1.2569	1.3016
3	0.5258	0.5684	3	1.2090	1.2467
4	0.5018	0.5538	4	1.1595	1.2009
5	0.4793	0.5235	5	1.1160	1.1650
6	0.4523	0.5167	6	1.0681	1.1057
7	0.4283	0.4738	7	1.0216	1.0700
8	0.4013	0.4375	8	0.9751	1.0168
9	0.3774	0.4209	9	0.9272	0.9599
10	0.3534	0.4151	10	0.8807	0.9321
11	0.3264	0.3600	11	0.8312	0.8668
12	0.3024	0.3513	12	0.7848	0.8451
13	0.2799	0.3390	13	0.7398	0.7757
14	0.2544	0.2872	14	0.6918	0.7380
15	0.2305	0.2729	15	0.6439	0.6906
16	0.2035	0.2352	16	0.5974	0.6300
17	0.1780	0.2271	17	0.5494	0.5908
18	0.1540	0.1979	18	0.5000	0.5486
19	0.1270	0.1784	19	0.4550	0.5091
20	0.1015	0.1377	20	0.4085	0.4504
21	0.0746	0.1288	21	0.3606	0.4083
22	0.0506	0.0883	22	0.3126	0.3558
23	0.0251	0.0739	23	0.2631	0.3263
24	-0.0004	0.0614	24	0.2152	0.2718
25	-0.0259	0.0164	25	0.1687	0.1946
26	-0.0513	-0.0037	26	0.1207	0.1621
27	-0.0768	-0.0478	27	0.0728	0.1196
28	-0.1023	-0.0632	28	0.0248	0.0692
29	-0.1292	-0.0795	29	-0.0262	0.0269
30	-0.1548	-0.0970	30	-0.0711	-0.0210
31	-0.1818	-0.1381	31	-0.1191	-0.0721
32	-0.2087	-0.1507	32	-0.1671	-0.1145
33	-0.2357	-0.1901	33	-0.2150	-0.1782
34	-0.2612	-0.2191	34	-0.2645	-0.2165
35	-0.2897	-0.2372	35	-0.3110	-0.2746
36	-0.3152	-0.2501	36	-0.3619	-0.3189

Table 4 - Continued

Comparison of Actual and Simulated Observations

	Span 1			Span 2	
Observation Number	Actual Range (+ 39269 km)	Simulated Range	Observation Number	Actual Range (+ 39255 km)	Simulated Range
37	-0.3391	-0.2967	37	-0.4099	-0.3626
38	-0.3661	-0.3111	38	-0.4594	-0.4170
39	-0.3931	-0.3367	39	-0.5058	-0.4606
40	-0.4216	-0.3743	40	-0.5553	-0.5215
41	-0.4471	-0.4091	41	-0.6048	-0.5586
42	-0.4726	-0.4265	42	-0.6557	-0.6057
43	-0.5010	-0.4549	43	-0.7007	-0.6619
44	-0.5295	-0.4778	44	-0.7502	-0.7028
45	-0.5550	-0.5015	45	-0.7996	-0.7503
46	-0.5820	-0.5414	46	-0.8491	-0.8088
47	-0.6105	-0.5636	47	-0.8986	-0.8482
48	-0.6359	-0.5869	48	-0.9465	-0.9001

3.4 Comparison of Actual and Simulated Observations

As previously stated, in this study simulated rather than actual observations are used. The simulated observables are created by adding random Gaussian noise to the 'true' observables determined using the true state from the ODPAC orbit simulator and the site coordinates. This noise can be adjusted by specifying the random seed (MRS) used to generate the noise and the standard deviation of the noise distribution (MNE). Letting MRS = 1019 and MNE = 7.62×10^{-3} km the simulated range observations obtained for the first two observation spans are as shown in Table 4. MRS was chosen by trial and error, while MNE was taken from [Brogan and Lemay, 1968]. While at first inspection the agreement between the actual and simulated range observations may not appear to be exceptional, a linear regression analysis yields a line

for the first (second) observation span, relating the simulated range to the actual range, with a slope of 1.0028 (0.9981) and a b-intercept of 0.0450 km (0.0425 km). Hence, except for a positive bias of less than 46 meters the simulated observations emulate the true observations very well. This conclusion is further supported by the correlation coefficients obtained during the linear regression analysis: 0.9994 for the ranges in observation span 1 and 0.9998 for the ranges in observation span 2. Finally, the mean and standard deviations (in km) for the actual and simulated ranges for observation span 1 are (39268.9806, 0.3609) and (30269.0255, 0.3621), respectively. For observation span 2, the corresponding values are (39255.1880, 0.6705) and (39255.2302, 0.6694).

The non-zero bias in the simulated range measurements is not unexpected given the errors cited in Fig. 1. To reach the end of observation span 2 ODPAC must simulate the orbit for over 2-1/2 hours. It is known from Fig. 1 that in this period of time, the spacecraft orbital radius vector predicted by ODPAC is ∿ 40 km in error compared to the accepted radius vector from the GTDS orbit simulator. It is not surprising, therefore, that the simulated observations based on the true state from ODPAC should have a bias of the same approximate magnitude.

4. THEORETICAL CONSIDERATIONS

The equations governing the extended Kalman filter are summarized in what follows, insofar as to highlight the quantities which can be varied to control the performance of the filter. Whenever possible, special forms for the various matrices, as related to the present problem of estimating a geostationary orbit using only range observations, are cited. In this regard the work of

17

[Brogan and Lemay, 1968] is most useful.

As stated in [Chodas, 1981], the Kalman filter equations can be divided into two sets. The first set is used to update the estimate and error covariance from time t_k to t_{k+1}:

$$\hat{\underline{x}}(k+1|k) = \hat{\underline{x}}(k|k) + \int_{t_k}^{t_{k+1}} \underline{f}[\hat{\underline{x}}(t, t_k), t]dt \qquad (4.1)$$

$$P(k+1|k) = \Phi(k+1, k)P(k|k)\Phi^T(k+1, k) + Q(k+1) \qquad (4.2)$$

Here, $\hat{x}(k|j)$, $P(k|j)$ and $\Phi(k|j)$ are the state estimate, the error covariance matrix and the state transition matrix at time t_k, given measurements to t_j. $Q(k)$ is the state noise matrix at t_k. The second set of equations improves the estimated state and error covariance matrix, given an observation at time t_{k+1}:

$$K(k+1) = P(k+1|k)H^T(k+1)[H(k+1)P(k+1|k)H^T(k+1) + R(k+1)]^{-1} \qquad (4.3)$$

$$\hat{\underline{x}}(k+1|k+1) = \hat{\underline{x}}(k+1|k) + K(k+1)[\underline{z}_{k+1} - h(\underline{x}(k+1|k), t_{k+1})] \qquad (4.4)$$

$$P(k+1|k+1) = [I - K(k+1)H(k+1)]P(k+1|k)[I - K(k+1)H(k+1)]^T$$

$$+ K(k+1)R(k+1)K^T(k+1) \qquad (4.5)$$

The Kalman gain matrix, the measurement matrix, the measurement noise matrix and the measurement vector at time t_k are denoted by $K(k)$, $H(k)$, $R(k)$ and $\underline{z}_k$, respectively. To initialize the filter an a priori state estimate $\hat{\underline{x}}_o$ and

its error covariance P_o,

$$P_o = E\{\hat{\underline{x}}_o \, \hat{\underline{x}}_o^T\} \qquad (4.6)$$

must be known. The notation $E\{\ \}$ denotes expectation. Also, the initial state noise matrix Q_o and the initial measurement noise matrix R_o must be specified. It is these three matrices which may most easily be varied to control the filter's performance.

4.1 The State Function and State Transition Matrix

The state function $\underline{f}$ forms the right-hand side of the state equation and describes the dynamics of the system:

$$\frac{d\underline{x}}{dt} = \underline{f}[\underline{x}(t), \, t] \qquad (4.7)$$

For a spacecraft orbiting a primary body under the influence of various perturbing accelerations, $\underline{f}$ takes on the form [Chodas, 1981]

$$\underline{f} = \left[v_x, \, v_y, \, v_z, \, -\frac{\mu}{r^3} x - a_x, \, -\frac{\mu}{r^3} y - a_y, \, -\frac{\mu}{r^3} z - a_z \right]^T \qquad (4.8)$$

when expressed in inertial coordinates. The state, in these same coordinates, is

$$\underline{x} = [x, \, y, \, z, \, v_x, \, v_y, \, v_z]^T \qquad (4.9)$$

The first three elements of (4.9) are the components of the orbital radius vector $\underline{r}$, while the second three elements are the components of the spacecraft's

19

velocity vector $\underline{v}$. They play a key role in the state function $\underline{f}$, as do the

perturbing accelerations $\underline{a}$, the components of which are given by

$$\underline{a} = [a_x, a_y, a_z]^T \qquad (4.10)$$

in inertial coordinates. The variable μ is the gravitational parameter of

the primary body

$$\mu = GM \qquad (4.11)$$

where G is the universal gravitational constant and M is the mass of the

attracting primary. Inertial coordinates are chosen here for ease of com-

parison with the GTDS run results. (For the chosen GTDS run, the equations

are integrated in inertial coordinates.) Other representations are possible,

however, and the interested reader is referred to [Chodas, 1981].

The state transition matrix $\Phi(t_{k+1}, t_k)$ used in ODPAC is approximated

by the matrix exponential:

$$\Phi(t_{k+1}, t_k) = e^{F\Delta t} \qquad (4.12)$$

where

$$F = \left. \frac{\partial \underline{f}}{\partial \underline{x}^T} \right|_{\underline{x}=\underline{\bar{x}}} \qquad (4.13)$$

and $\Delta t = t_{k+1} - t_k$. For the purpose of computing F, the perturbing accel-

erations $\underline{a}$ are neglected in (4.8). The result is

$$F = \begin{bmatrix} 0 & I \\ -\dfrac{\mu}{r^3}\left(I - \dfrac{3}{r^2}\,\underline{r}\,\underline{r}^T\right) & 0 \end{bmatrix} \qquad (4.14)$$

20

Equation (4.13) is based on a linearization of (4.8) about some reference state $\underline{x} = \bar{\underline{x}}$. In general, this reference state is taken to be the current best estimate of the true state. For the present problem, that of a space-craft in 'geostationary' orbit, the most appropriate reference state is an ideal geostationary orbit. [In reality, disturbing forces (modeled by $\underline{a}$) force the satellite from the ideal, hence the quotation marks.] A closed-form transition matrix based on this realization is derived in Appendix A [Brogan and Lemay, 1968]. While the state transition matrix used in ODPAC does not have this form by design, it should still approximate the matrix given in Appendix A, provided the reference about which (4.8) is linearized is a geostationary orbit. As stated above this is not, in fact, the case. However, the state transition matrix from ODPAC was verified numerically to have a form very similar to that given in Appendix A. In particular, elements of Φ which should have been zero were typically at least an order of magnitude less than elements which were expected to be nonzero. It is not clear at this juncture whether modifying ODPAC to use the closed-form state transition matrix to predict very nearly geostationary orbits would improve the filter's performance. In any case, such a modification to the program was considered beyond the scope of the present study and not attempted.

4.2   The Measurement Function and Measurement Matrix

The measurement function $\underline{h}$ depends on the type of measurements to be made, the coordinates of the observing sites, the model assumed for the Earth and the equations required to compute predicted observations from the position and velocity coordinates of the satellite. The permitted elements for the measurement vector z,

$$z = \underline{h}[\underline{x}(t), t] \qquad (4.15)$$

with regard to ODPAC, are azimuth, elevation, range and range rate. Here, we are interested only in range; however, the form of $\underline{h}$ is still relatively complicated, even for this measurement. For details, the interested reader is referred to Chapter 5 of [Chodas, 1981].

In a manner analogous to the linearization of the state function, the measurement matrix H is obtained by linearizing $\underline{h}$ about some reference state $\underline{x} = \underline{\bar{x}}$. The result is

$$H = \left. \frac{\partial \underline{h}}{\partial \underline{x}^T} \right|_{\underline{x} = \underline{\bar{x}}} \qquad (4.16)$$

Again, the chosen reference state is the best current estimate of the true state. When only range measurements are considered H has the simple form

$$H = \left[\frac{1}{\rho} \underline{\rho}^T, \ 0, \ 0, \ 0 \right] \qquad (4.17)$$

where the range $\underline{\rho}$, expressed in inertial coordinates, is

$$\underline{\rho} = [\rho_x, \ \rho_y, \ \rho_z]^T \qquad (4.18)$$

As a point of clarification, $\underline{h}[\underline{x}(k+1|k), t_{k+1}]$ in (4.4) computes the predicted measurements, while the elements of $\underline{z}_{k+1}$ are actual measurements, or, as is the case here, simulated measurements.

4.3 The State Noise and Measurement Noise Matrices

Normally the choice of state noise and measurement noise matrices falls

into the realm of a knowledgeable guess or a trial-and-error search to find acceptable performance. For the present problem, where only range is observed, the measurement noise matrix has only one scalar entry, the variance in the range anticipated because of noisy measurements:

$$R(k) = \sigma_\rho^{\ 2} \qquad\qquad (4.19)$$

However, the value to assign to σ_ρ is still in question. A number of values have been suggested in the literature, but a value of $\sigma_\rho = 25$ ft $(7.62 \times 10^{-3}$ km) is typical.

For a geostationary reference orbit, considerable progress can be made in predicting the portion of $Q(k)$ attributed to neglecting _a_ in computing the state transition matrix [recall (4.12)]. Again, the work of [Brogan and Lemay, 1968] is of interest. Appendix B highlights their derivation and culminates in the analytical prediction of $Q(k)$ based on unmodeled accelerations. Conceivably, $Q(k)$ can also have a component based solely on random noise. While this is a useful area for future study, for the present, the performance of the ODPAC Kalman filter will be assessed using the $Q(k)$ matrix given in Appendix B alone. This matrix is a function of the time interval Δt, the angular velocity of an ideal geostationary orbit ω and the variance in the unmodeled accelerations $\sigma_a^{\ 2}$. As for the range variance, a typical value of $\sigma_a = 10^{-7}$g $(9.80650 \times 10^{-10}$ km/sec$^2)$ is adopted, based on the literature. Care must be exercised when using the Brogan Q matrix to recompute and enter a new Q each time the state update interval Δt is changed.

From the viewpoint of filter performance, once the state update schedule has been specified, the quantities which can be varied to improve performance are σ_ρ and σ_a.

4.4 The Error Covariance Matrix

As stated earlier, the error covariance matrix corresponding to the initial estimated state must be specified to initialize the Kalman filter (4.6). Unfortunately, the variances and covariances of the individual components of the estimated state are not known in advance. As a consequence, once again the best that can be done is to estimate P_o. For equations integrated in inertial coordinates, what is typically done is to predict the position error DR and velocity error DV of the initial estimated state. P_o is then chosen to be diagonal with DR^2 forming the first three elements along the diagonal and DV^2 forming the remaining three. In practice, the problem is to determine DR and DV:

$$DR = [(x-\hat{x})^2 + (y-\hat{y})^2 + (z-\hat{z})^2]^{\frac{1}{2}} \qquad (4.20)$$

$$DV = [(v_x-\hat{v}_x)^2 + (v_y-\hat{v}_y)^2 + (v_z-\hat{v}_z)^2]^{\frac{1}{2}} \qquad (4.21)$$

We know the true state (x, y, z, v_x, v_y, v_z) from the GTDS results, as well as the initial estimated state $(\hat{x}, \hat{y}, \hat{z}, \hat{v}_x, \hat{v}_y, \hat{v}_z)$. Hence DR and DV are known exactly for our purposes. However, to add some of the uncertainty present in a real system the exact values are not used, but rather DR^2 and DV^2 are rounded to the nearest km^2 and $(km/sec)^2$. The adopted values, based on the chosen GTDS run (Section 3.1), are $DR^2 = 13$ km^2 and $DV^2 = 6\times10^{-8}$ $(km/sec)^2$.

The freedom to choose DR and DV initially, even though the 'true' values are known, provides yet another parameter which can be varied to affect the filter's performance, at least in the initial stages of the estimation. Also, the technique of diagonalizing P at the end of the first estimation step

24

during which observations were processed [Browne and McPherson, 1978(2)] can be employed to affect filter performance. ODPAC [McPherson and Copeck, 1980] accomplishes this by use of a scalar variable NDPK. Let the update interval be Δt and current estimation time be T, then for NDPK$\cdot\Delta t \leqq$ T the off-diagonal elements of P are set to zero, while for NDPK$\cdot\Delta t >$ T P remains unchanged. To accomplish the desired diagonalization at time T_1 (the T value at which the first observation is processed) one must set NDPK = T_1 immediately after time $T_1-\Delta t$ (i.e., just before the next update step to T_1). ODPAC's interactive mode facilitates this by use of an ENT command immediately after a RUN command to $T_1-\Delta t$ and prior to a RUN command to T_1.

5. NUMERICAL STUDIES

The performance of the Kalman filter is first established for an orbit that has an initial true state which, in the absence of perturbative accelerations, describes an ideal geostationary orbit. The filter's performance is then tested using the initial true state from the chosen GTDS run, which does not define an ideal geostationary orbit. In all these studies the state noise matrix is assumed to have the form given in Appendix B. Furthermore, the initial error covariance matrix P_o is always diagonal. The state transition matrix is unchanged from that assumed in ODPAC.

5.1 Run Schedule and Baseline Values

To make comparison between the various numerical studies more meaningful a standard run schedule was adopted for all the runs. This schedule was designed to incorporate the period of time containing the first two

observation spans from the GTDS run. While it was felt that the filter's tendency to converge or diverge could adequately be assessed based on this four-hour period, this choice was dictated more by the sim-file limitations within ODPAC. These files store a simulated true-state run rather than re-generating it each time. Even after optimizing the space by choosing non-uniform update times Δt, a run duration of only a little better than four hours could be achieved. Initially, the time required to interact with ODPAC was also prohibitive because each time Δt was changed Q (6×6) also had to be modified and re-entered. This problem was later averted by running ODPAC in a batch mode with an input file equivalent to all the interactive commands necessary during an on-line run. In retrospect, the batch mode offers a convenient way to extend the four-hour run duration by, in fact, re-generating the true state trajectory each time. This was not attempted in the inter-active mode where the problem of recomputing and re-entering Q five times per run consumed enough time, so that longer runs were totally impractical. Table 5 contains the chosen run schedule and highlights the important events.

Baseline values for P_o, R and Q were given in Chapter 4; however, for ease of referral they have been collected and summarized in Table 6. The initial error covariance and measurement noise matrices are input only once at the beginning of each run, while the state noise matrix must be re-entered each time Δt changes. As a consequence, there are, in fact, four baseline state noise matrices, one for each different update interval in Table 5. These matrices must be computed externally from ODPAC, but need be computed only once. Finally, ODPAC actually requires Q' (see Table 6) and not Q, as the state noise matrix is multiplied by Δt within the program.

Table 5

Run Schedule

Time (sec)	Update Interval (sec)	Events
0		- corresponds to TO=44,058.5, the Epoch date from the GTDS run
	517	- input true and estimated state
		- input P_o, R, Q' (see Appendix B)
5170		- step prior to first observation; when diagonalizing P, NDPK = 518 entered immediately after this time
	10	- input a new Q' because Δt changes
5180		- first observation span encountered; update interval chosen to match actual GTDS observations
	10	
5650		- first observation span terminated
	10	
5660		- for plotting purposes compute state at first point after observation span
	323	- input a new Q' because Δt changes
8890		- second observation span encountered; again, update interval chosen to match GTDS observations
	10	- input a new Q' because Δt changes
9370		- second observation span terminated
	10	
9380		- for plotting purposes compute state at first point after observation span
	509	- input a new Q' because Δt changes
14470		- terminate run at what would be the beginning of the third observation span

Table 6

Baseline Values

Initial Error Covariance Matrix

$$P_O = \text{diag}\{DR_B^2,\ DR_B^2,\ DR_B^2,\ DV_B^2,\ DV_B^2,\ DV_B^2\}$$

$$DR_B^2 = 13\ \text{km}^2; \quad DV_B^2 = 6\times10^{-8}\ (\text{km/sec})^2$$

Measurement Noise Matrix

$$R = [\sigma_{\rho B}^2]$$

$$\sigma_{\rho B} = 7.62\times10^{-3}\ \text{km}$$

State Noise Matrix

$$Q = Q'\Delta t = \sigma_{aB}^2 \begin{bmatrix} \Delta t^4/4 & 0 & 0 & \Delta t^3/2 & -\omega\Delta t^4/2 & 0 \\ & \Delta t^4/4 & 0 & \omega\Delta t^4/2 & \Delta t^3/2 & 0 \\ & & \Delta t^4/4 & 0 & 0 & \Delta t^3/2 \\ & & & \Delta t^2(1+\omega^2\Delta t^2) & 0 & 0 \\ & (\text{sym}) & & & \Delta t^2(1+\omega^2\Delta t^2) & 0 \\ & & & & & \Delta t^2 \end{bmatrix}$$

$$\sigma_{aB} = 9.806650\times10^{-10}\ \text{km/sec}; \quad \Delta t = (10,\ 517,\ 323,\ 509)$$

5.2 Filter Performance for an Ideal Geostationary Orbit

A series of runs was conducted to assess the ability of the ODPAC Kalman estimator to determine the orbit of a spacecraft which, in the absence of external disturbances, would move exactly in a geostationary orbit. These runs were also used to assess the importance of selecting different perturbations in the orbit (true-state) simulator and the orbit estimator. Finally, the effect of diagonalizing P after processing the first observation was also studied. A total of eight runs was conducted: one set of four in which P was not diagonalized, and a second set of four in which it was diagonalized. The baseline values for P_o, R and Q were assumed in all the runs. To assess the effect of neglecting different perturbations in the simulator and the estimator, the extreme point of view was taken. Simply, all the perturbations were neglected in either the simulator or the estimator. These two cases formed the second and third run in each four-run set. The first run in each set included all of the perturbations cited in Chapter 2 in both the simulator and the estimator. The fourth run neglected the perturbations in both the simulator and the estimator. While this last run may appear somewhat useless in that it should reproduce the results of the first run (assuming the perturbation models used in both the estimator and the simulator are identical--and they are, in fact, analytically) preliminary runs did not give this result. It was found by searching through the possible perturbation models that the correction for precession and nutation was not correctly implemented in the ODPAC estimator software. This situation was corrected by W. B. Graham at the Communications Research Centre so that this discrepancy no longer appears on the plots resulting from this study.

29

To ensure the ODPAC simulator produced a true-state trajectory that was indeed geostationary a separate ephemeris run was conducted without any estimation. The initial true state (TST) was entered to 17 significant digits to ensure the highest possible accuracy:

$$
TST = \begin{bmatrix} 42164.182266336229 \\ 0 \\ 0 \\ 0 \\ 3.0746610200852333 \\ 0 \end{bmatrix} \tag{5.1}
$$

Based on (5.1) the ODPAC orbit simulator simulated very accurately a geostationary orbit.

The initial estimated state (EST) was constructed by adding the position and velocity error implied by the true state and estimated state from the GTDS case run to the first and second non-zero entries in (5.1):

$$
EST = \begin{bmatrix} 42167.761761866179 \\ 0 \\ 0 \\ 0 \\ 3.0749065913490372 \\ 0 \end{bmatrix} \tag{5.2}
$$

This ensures that using the baseline P_O is sensible in this case and that the initial difference between the true and estimated states is consistent for all the numerical studies. The observations used are the simulated range measurements from Chapter 3.

The results from the set of runs in which P was not diagonalized are given in Fig. 3, while those in which P was diagonalized are shown in Fig. 4. The appearance of the letter E (S) signifies that the estimator (simulator) includes orbital perturbations. Each observation
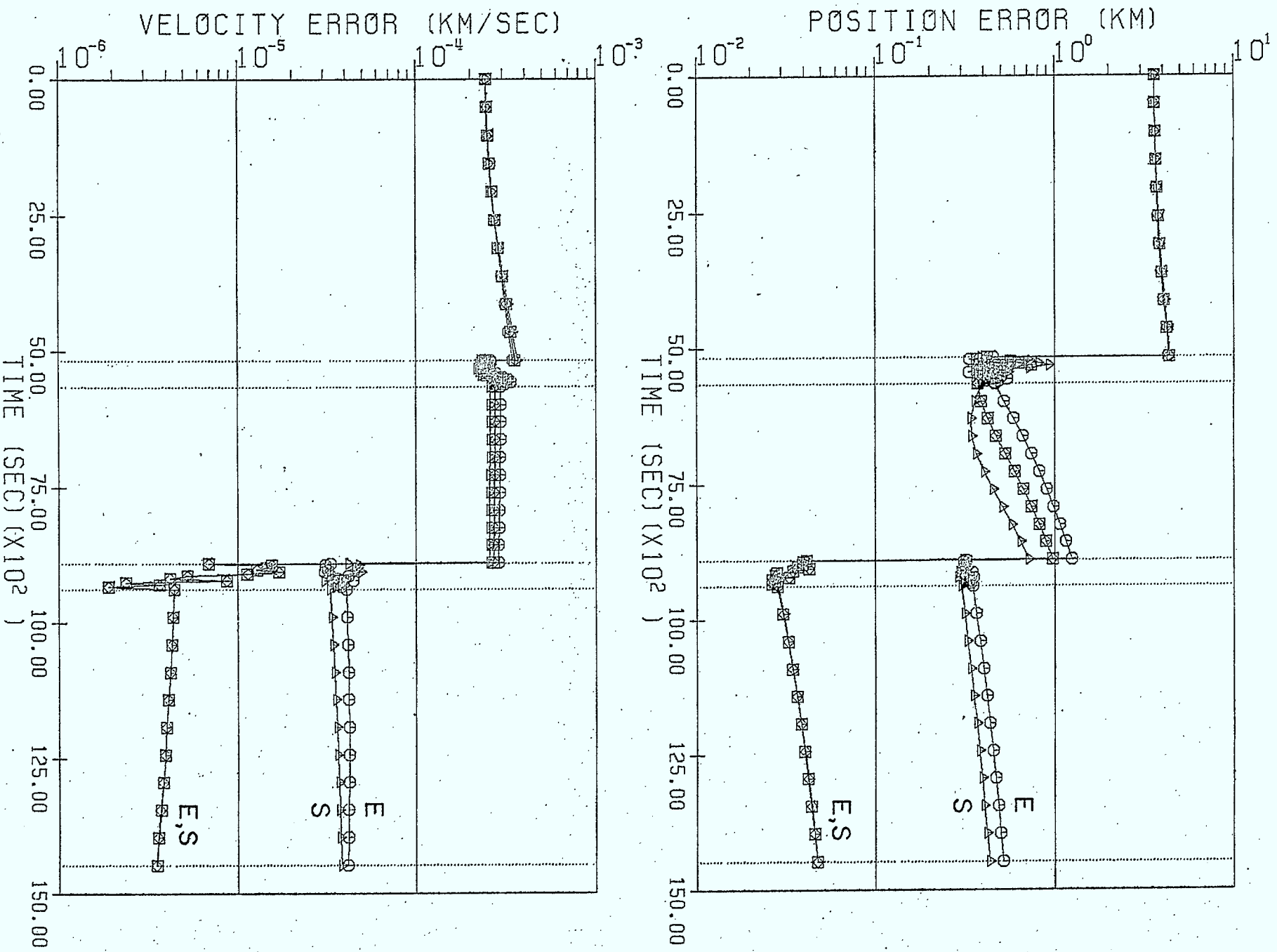
30

FIGURE 3. FILTER PERFORMANCE FOR AN IDEAL GEOSTATIONARY ORBIT
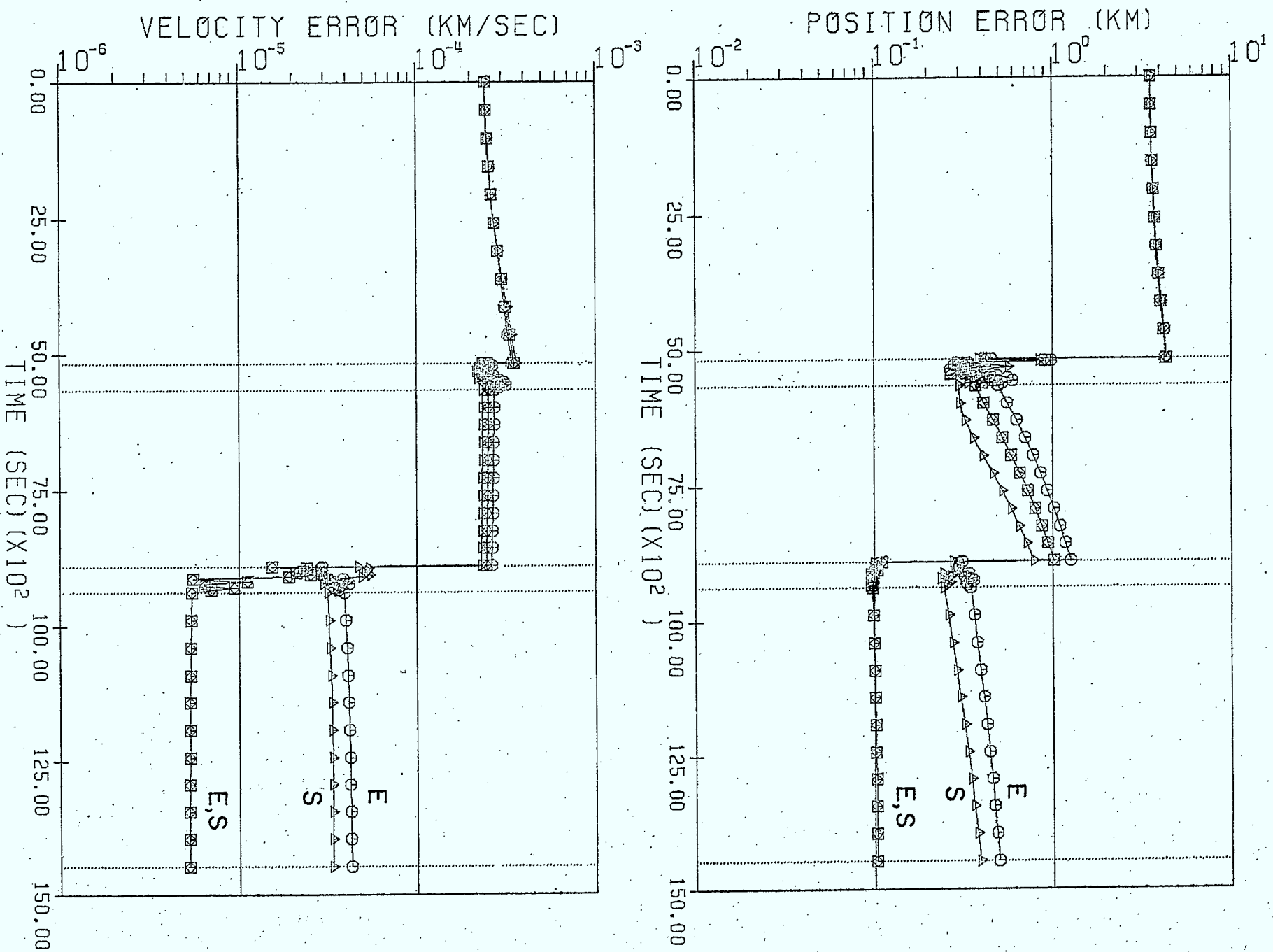(P NOT DIAGONALIZED).

31

FIGURE 4. FILTER PERFORMANCE FOR AN IDEAL GEOSTATIONARY ORBIT (P DIAGONALIZED).

32

span is indicated in the figures by two dotted lines forming a narrow vertical column across the plot. The terminal run-time is indicated by a single dotted vertical line.

The most significant feature about Figs. 3 and 4 is that the filter is converging. The best performance (an order of magnitude better) occurs when both the simulator and estimator have identical perturbation models (either all or none of the perturbations included). Surprisingly, the runs in which P is not diagonalized after processing the first observation, for the most part, outperform those in which it is diagonalized. Also, it appears from the plots that it is more crucial for the simulator to have the better perturbation model because the filter performs better when only the simulator includes perturbations. When only the estimator includes the perturbations, the performance degrades. This is to be expected, since the estimator essentially has a 'poorer' model for what the true state (as given by the simulator) will be. The convergence evident in both figures is very encouraging and supports the belief that the chosen P_o, R and Q matrices might be suitable for an 'almost' geostationary orbit.

5.3   Filter Performance for an Approximately Geostationary Orbit

The approximate geostationary orbit chosen is that of the GTDS run cited in Section 3.1. The initial true state and estimated state (in inertial coordinates) are inferred from that run:

$$
\text{TST} = \begin{bmatrix} 40845.37213829510 \\ -10615.73853774204 \\ -872.8259802956517 \\ 0.7722841035999041 \\ 2.973490590000106 \\ -0.009800138752845655 \end{bmatrix} ; \quad \text{EST} = \begin{bmatrix} 40844.60517000308 \\ -10618.58727000253 \\ -874.8531143380704 \\ 0.7720479004666814 \\ 2.973554475773058 \\ -0.009779355762572144 \end{bmatrix} \quad (5.3)
$$

33

$$DR = 3.5794955300 \text{ km}; \quad DV = 2.4557126229 \times 10^{-4} \quad (5.4)$$

Ideally, the third (z) and sixth (v_z) elements in the true state vector should be identically zero for a geostationary orbit. The observations used in this study are the simulated ranges given in Chapter 3.

Preliminary runs using the baseline values for P_o, R and Q result in a performance much different than that shown in Figs. 3 and 4. The filter diverges very marginally in velocity, achieving a value of $DV = 2.526 \times 10^{-4}$ km/sec at the end of the scheduled run. However, it converges very marginally in position to a value of DR = 3.277 km over the same period. Furthermore, the filter performs slightly worse than when P is not diagonalized after the first observation, giving values of $DR = 3.297$ km and $DV = 2.568 \times 10^{-4}$ km/sec at run termination.

In an effort to determine if the filter performance could be improved by simply varying the filter's parameters (the elements in P_o, R and Q) rather than the actual forms of the matrices themselves, an extensive parameter study was performed. The elements of R and Q were varied by approximately six orders of magnitude (in increments of 10) about their baseline values. DR and DV were varied by approximately four orders of magnitude about their baseline values (in increments of 100). The variations in DR and DV may appear rather coarse initially; however, they are adequate to establish trends. Furthermore, as is shown in the parameter variation summary given in Table 7, this choice generates a reasonably large number of runs. The possibility of having zero measurement error, zero state error, zero position error or zero velocity error was also explored.

34

Table 7

Parameter Variation Summary

(for NDPK = 0 and for NDPK = 518)

Initial Error Covariance Matrix

DV km/sec	DR^2 / DV^2	DR km → 0 / 0	10^{-4} / 10^{-8}	10^{-2} / 10^{-4}	1 / 1	10^2 / 10^4	10^4 / 10^8	
0	0	P1	P2	P3	P4	P5	P6	
10^{-8}	10^{-16}	P7	P8	P9	P10	P11	P12	
10^{-6}	10^{-12}	P13	P14	P15	P16	P17	P18	Q and R at baseline values
10^{-4}	10^{-8}	P19	P20	P21	P22	P23	P24	
10^{-2}	10^{-4}	P25	P26	P27	P28	P29	P30	
1	1	P31	P32	P33	P34	P35	P36	

Approximately baseline value (row 10^{-4} / 10^{-8})

Run Numbers

Measurement Noise Matrix

σ_ρ km	0	10^{-7}	10^{-6}	10^{-5}	10^{-4}	10^{-3}	10^{-2}	10^{-1}	1	10	10^2	10^3
Run Number	R1	R2	R3	R4	R5	R6	R7	R8	R9	R10	R11	R12

Approximately baseline value   P and Q at baseline values

State Noise Matrix

σ_ρ km/sec^2	0	10^{-15}	10^{-14}	10^{-13}	10^{-12}	10^{-11}	10^{-10}	10^{-9}	10^{-8}	10^{-7}	10^{-6}	10^{-5}
Run Number	Q1	Q2	Q3	Q4	Q5	Q6	Q7	Q8	Q9	Q10	Q11	Q12

For Δt = (10, 517, 323, 509)   Approximately baseline value   P and R at baseline values

---

The results of the parameter study conducted on the initial error covariance matrix show some interesting trends. Runs P4, P10, P16, P19, P20, P21 and P22 show results very similar to the baseline run. Runs (P1, P2, P3), (P7, P8, P9), (P13, P14, P15) and (P19, P20, P21) all yield results which are also essentially the same as the baseline run. Therefore, choosing $[DR \leq DR_B$ and $DV \leq DV_B]$, where (DR_B, DV_B) are the baseline (DR, DV) values, will not change the filter performance substantially from that observed when the baseline P_o matrix is used. These (DR, DV) values correspond to the upper left-hand portion of the covariance run summary in Table 7. Figure 5 is typical of the run-triplets cited above. The baseline run (square plotting symbols) and three other runs (P13, P14, P15) are shown in the figure (round, triangle and diamond plotting symbols, respectively). This plotting format, showing the baseline plus three other runs, will be maintained for all remaining plots. From the figure it is apparent that each of the three plotted runs in fact outperforms the baseline run, but only marginally. The performance is not at all similar to that observed in Figs. 3 and 4.

It was also noted that runs (P5, P6), (P11, P12), (P17, P18) and (P23, P24), corresponding to $[DR > DR_B$ and $DV \leq DV_B]$, were very similar in character. Figure 6 is typical of these runs. Both runs P17 and P18 show divergent behaviour, as did all runs in this region. The remaining two regions of the covariance run summary shown in Table 7, $[DR \leq DR_B$ and $DV > DV_B]$ and $[DR > DR_B$ and $DV > DR_B]$, show erratic behaviour, with divergence always occurring in either the position or velocity error. Figures 7 and 8 (P25, P26, P27 and P28 in the former region, P29 and P30 in the latter) show typical results for these two regions.
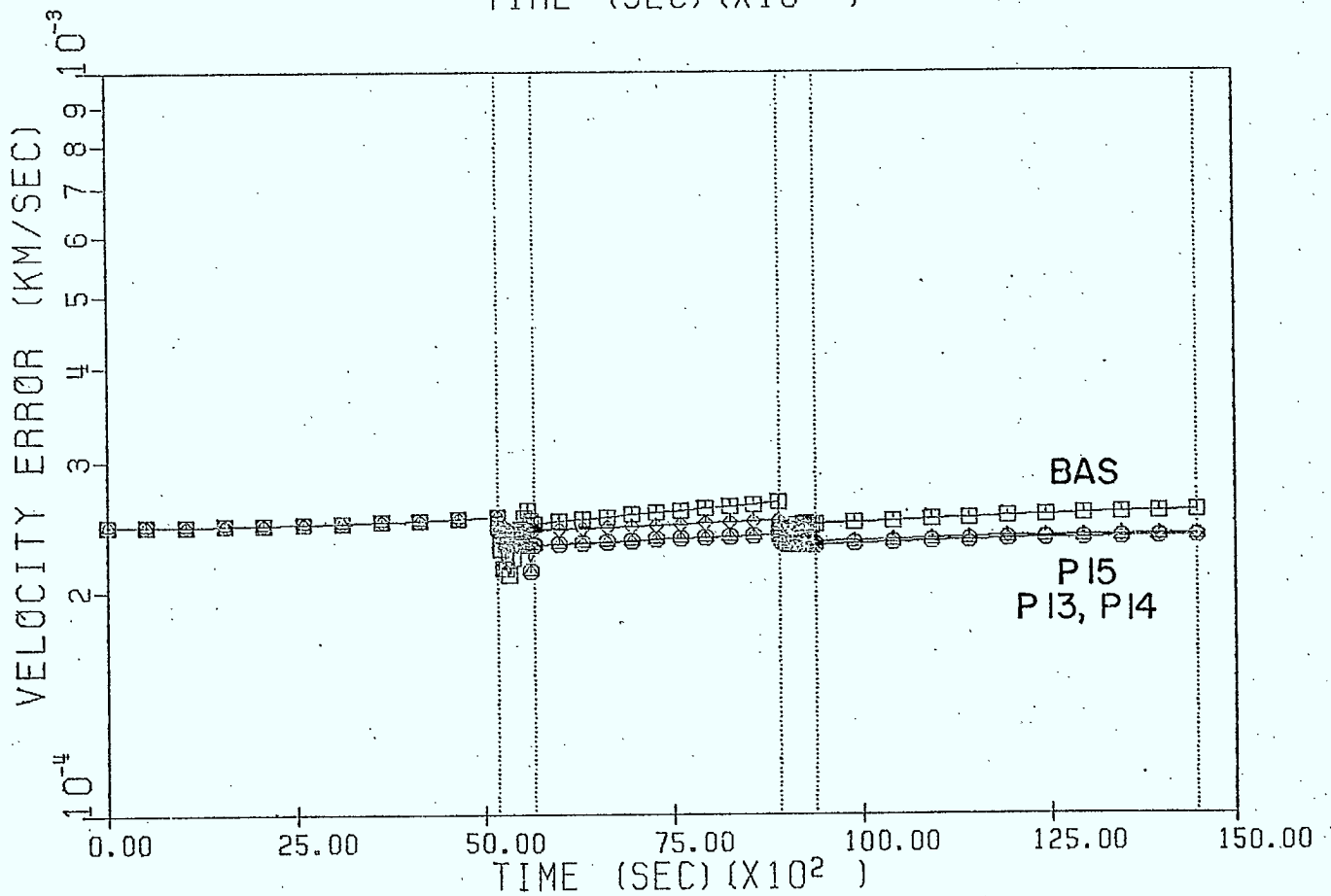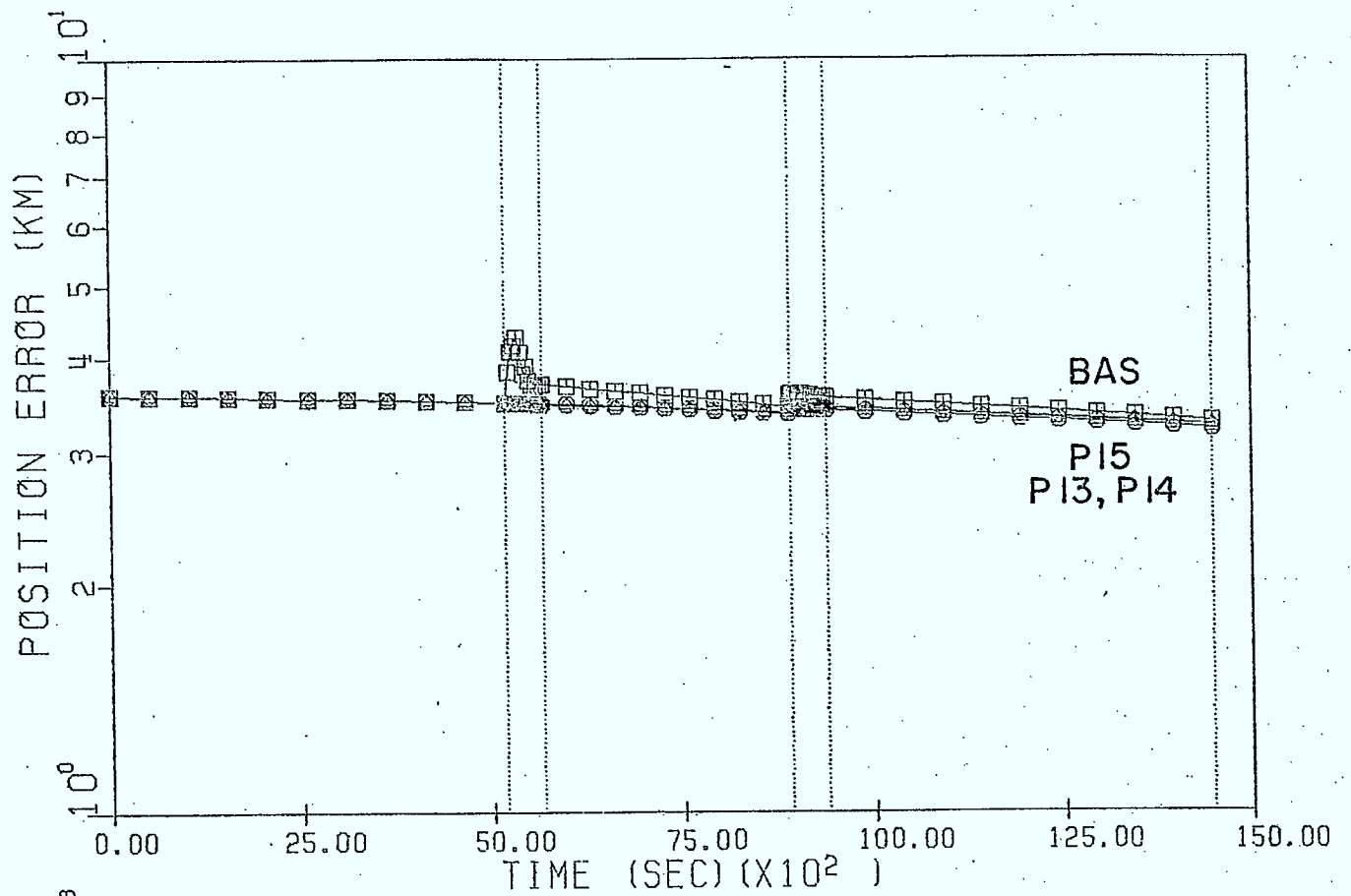
36

FIGURE 5. TYPICAL PERFORMANCE WHEN BOTH DR AND DV ARE BELOW
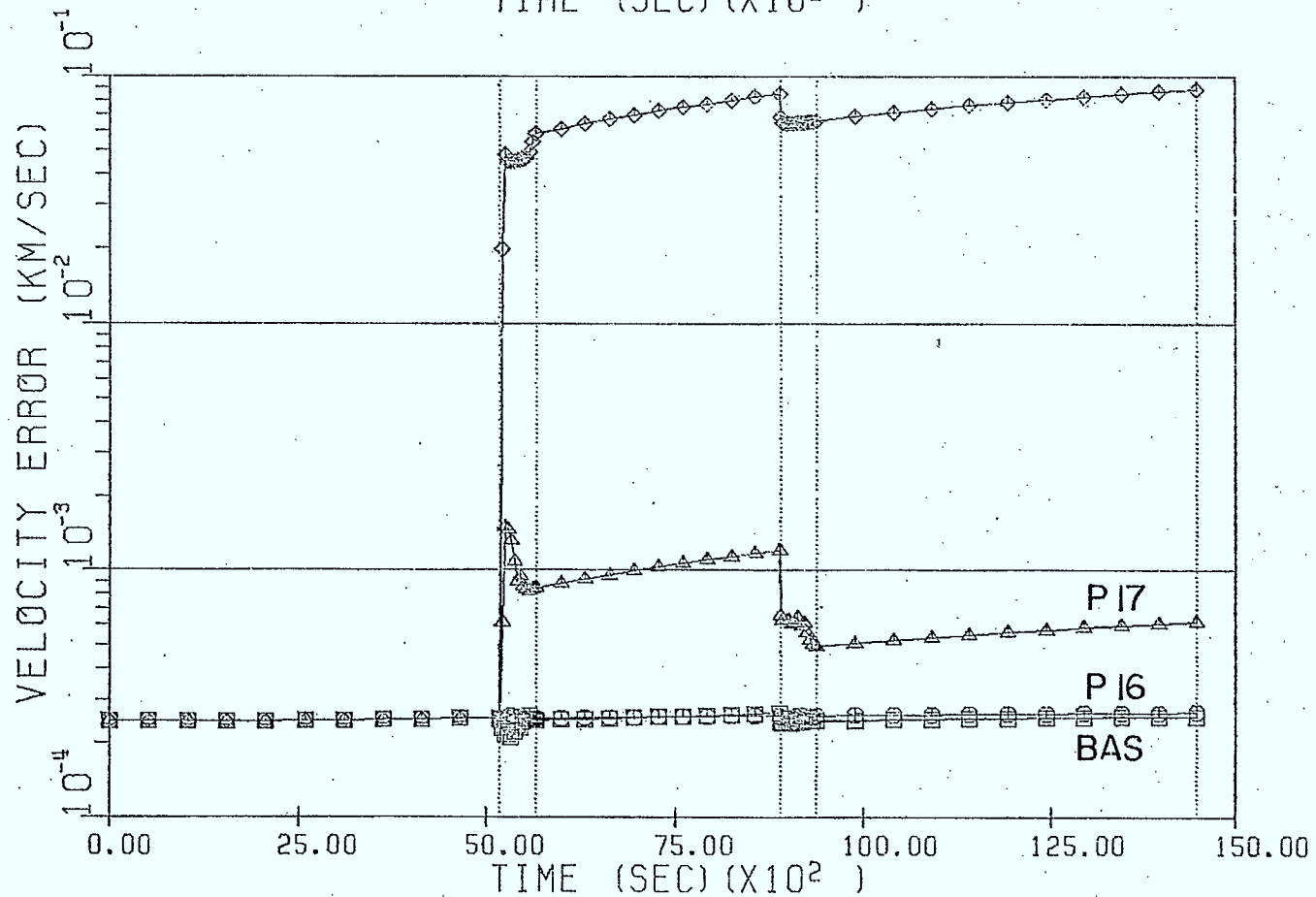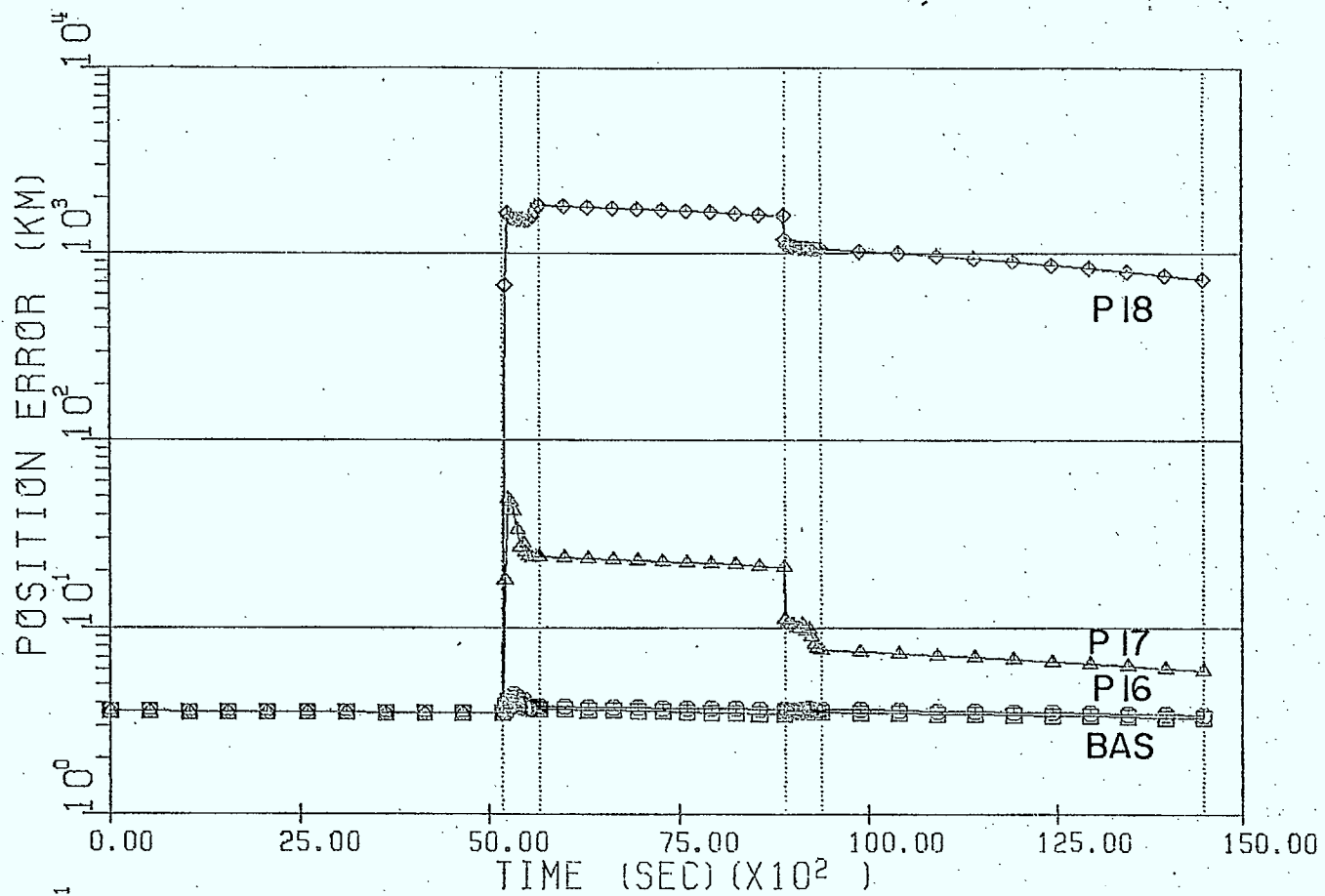THE BASELINE VALUES.

37

FIGURE 6. TYPICAL PERFORMANCE WHEN DR IS ABOVE AND DV IS BELOW
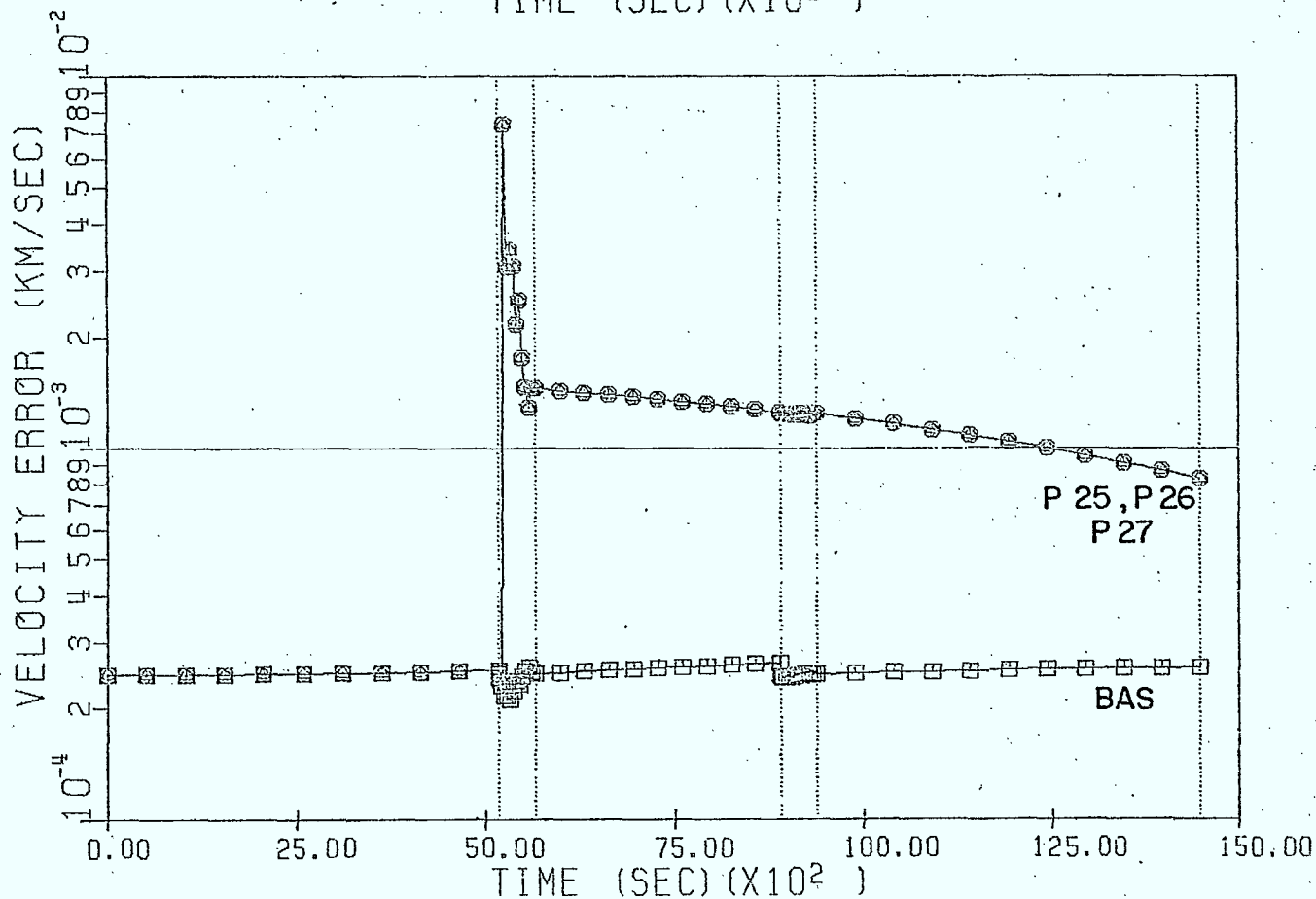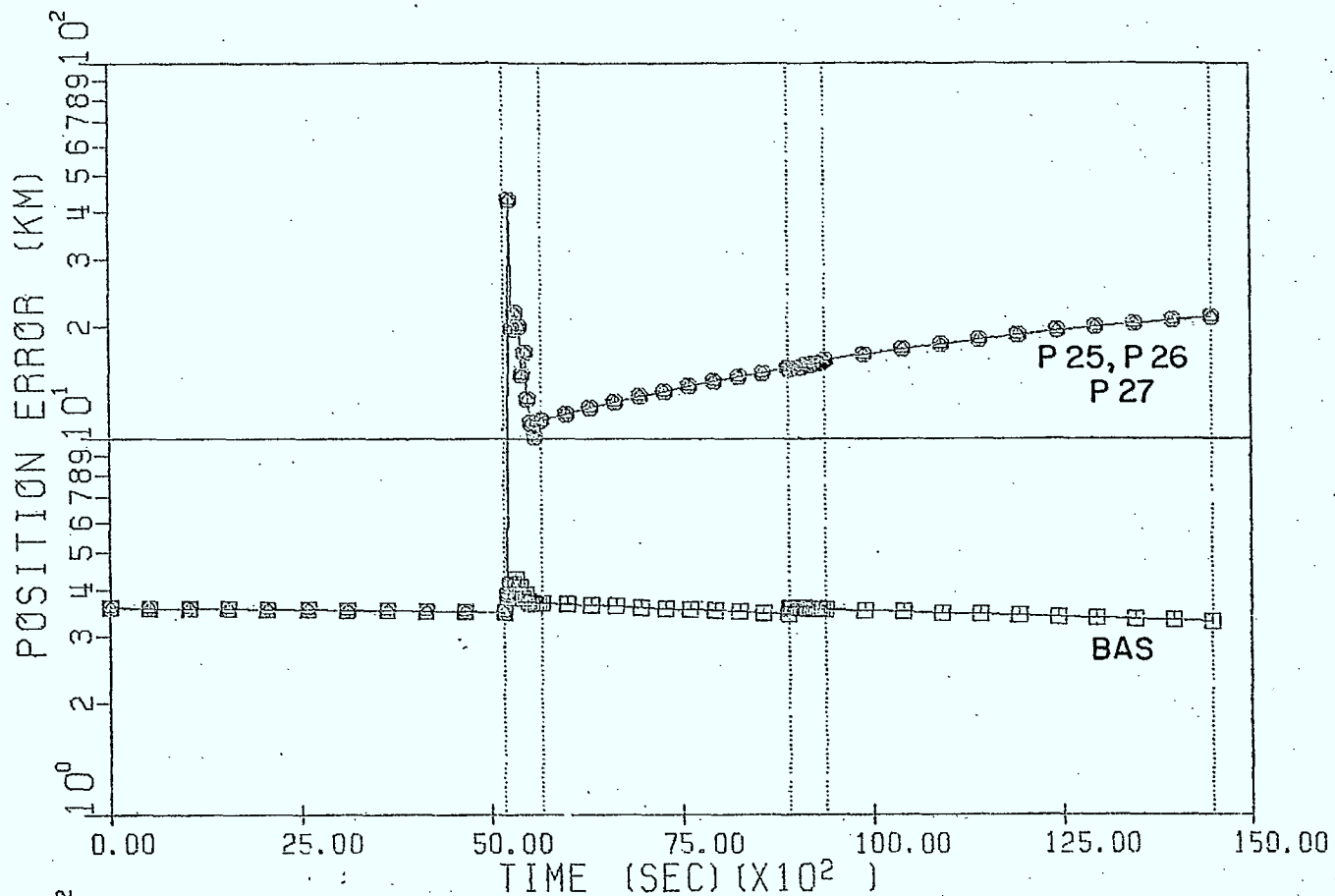THE BASELINE VALUES.

38

FIGURE 7. TYPICAL PERFORMANCE WHEN DR IS BELOW AND DV IS ABOVE
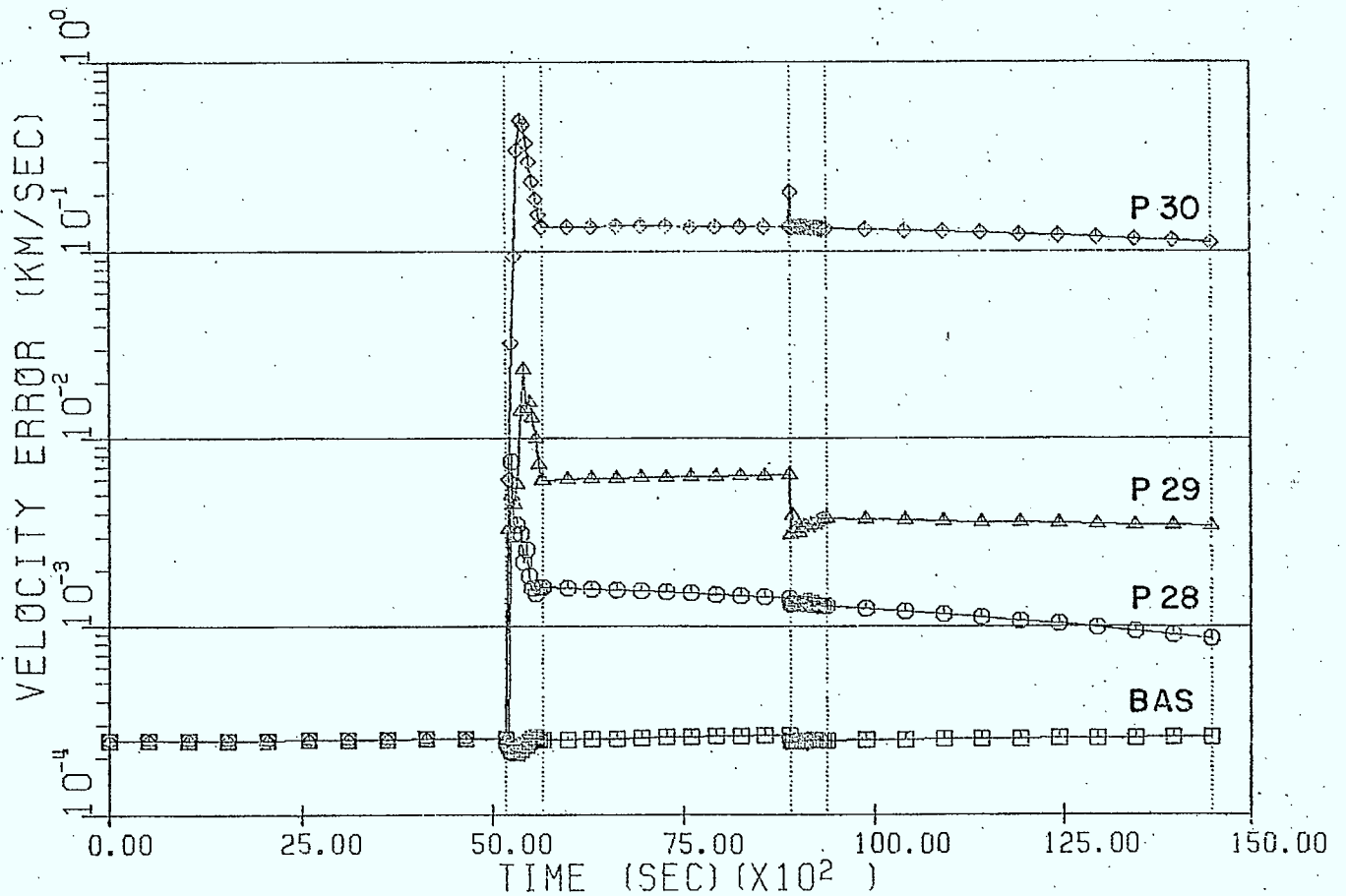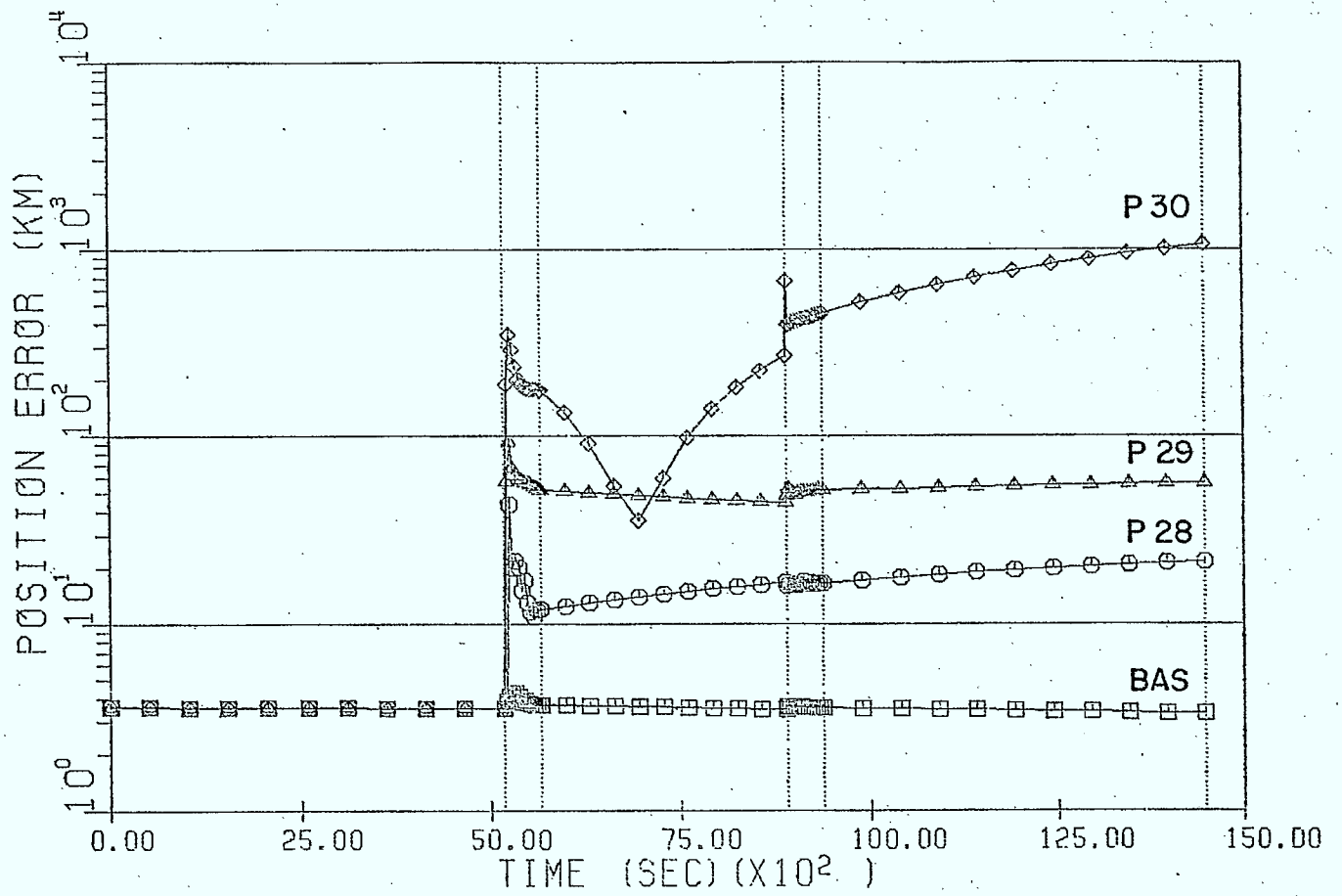THE BASELINE VALUES.

FIGURE 8. TYPICAL PERFORMANCE WHEN BOTH DR AND DV ARE ABOVE THE
BASELINE VALUES (EXCEPT RUN P28).

40

Figures 6 through 8 all represent cases in which P was not diagonal-ized after processing the first observation. When this diagonalization is performed no substantial difference is noted in the final position and velocity errors for the region [DR $\leq$ DR$_B$ and DV $\leq$ DV$_B$]. However, for the other regions the divergence is often more than an order of magnitude greater. Also, the error histories, while similar in the respective regions cited above, are often quite different from those in which P is diagonalized. Regardless, the results of the initial-error-covariance parameter study suggest that the filter performance cannot be improved substantially by simply varying P$_o$ through changes in DR and DV.

As for the covariance matrix parameters, a clear division of the filter performance is observed depending on whether the measurement noise deviation σ_ρ is above or below the baseline value, $\sigma_{\rho B}$. Figure 9 is typical of the results obtained for $\sigma_\rho < \sigma_{\rho B}$. The most interesting run is R6. It initially shows divergent behaviour, yet by the end of the run it yields position and velocity errors marginally less than those using the baseline parameters. The remaining runs in this region show divergent behaviour in either the position or the velocity error.

For $\sigma_\rho > \sigma_{\rho B}$, the performance of the filter is virtually unchanged from that using the baseline value. Figure 10 illustrates this finding. Once again, it would appear that varying the measurement noise will not greatly enhance the performance of the filter. Also once again, diagonal-ization of P after processing the first observation actually yields poorer results, except for runs R1 and R2 which are unstable (a diagonal element of P becomes negative) when P is not diagonalized.

The results of the previous two parameter studies suggest that the baseline values for DR, DV and σ_ρ are well chosen. The results from the
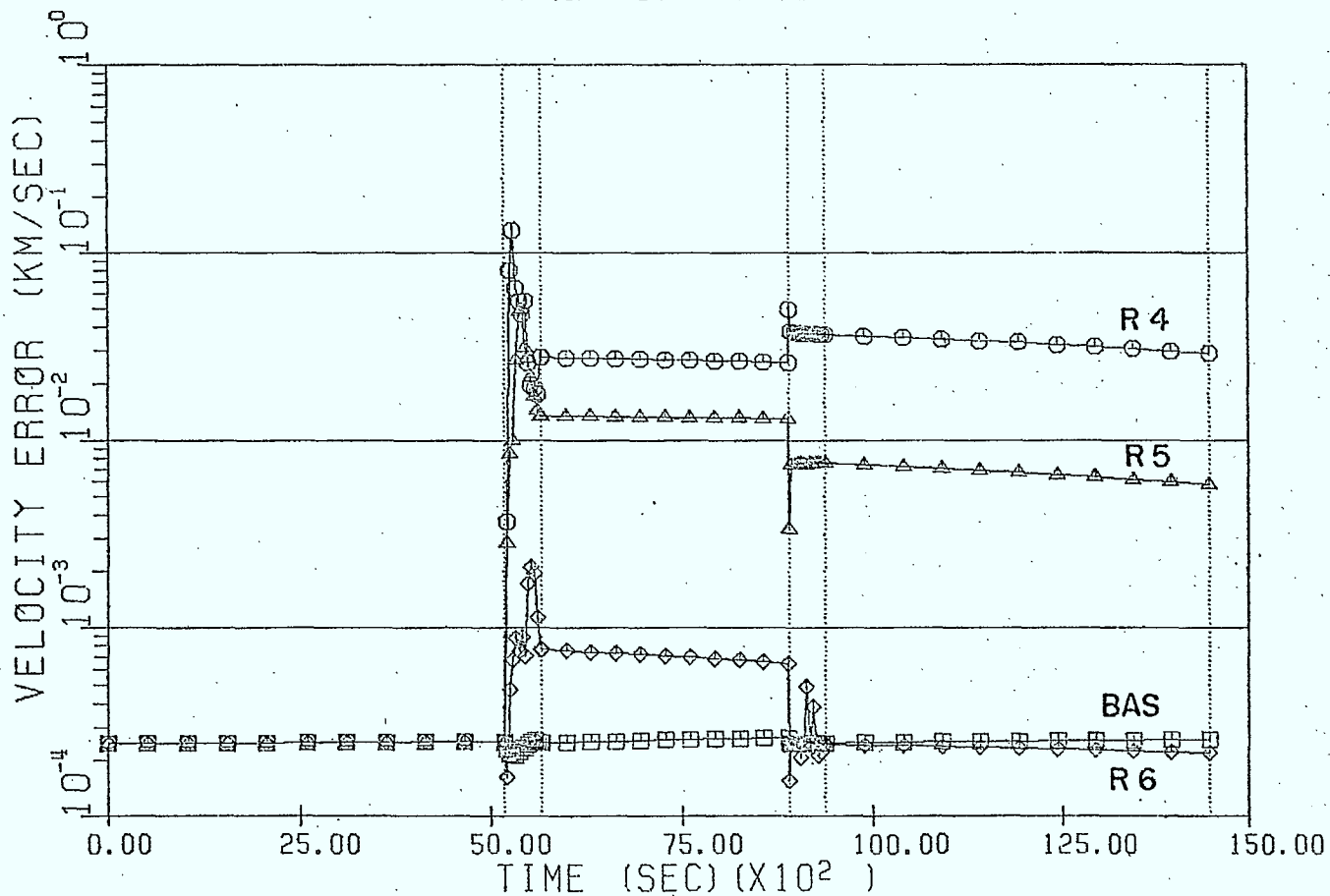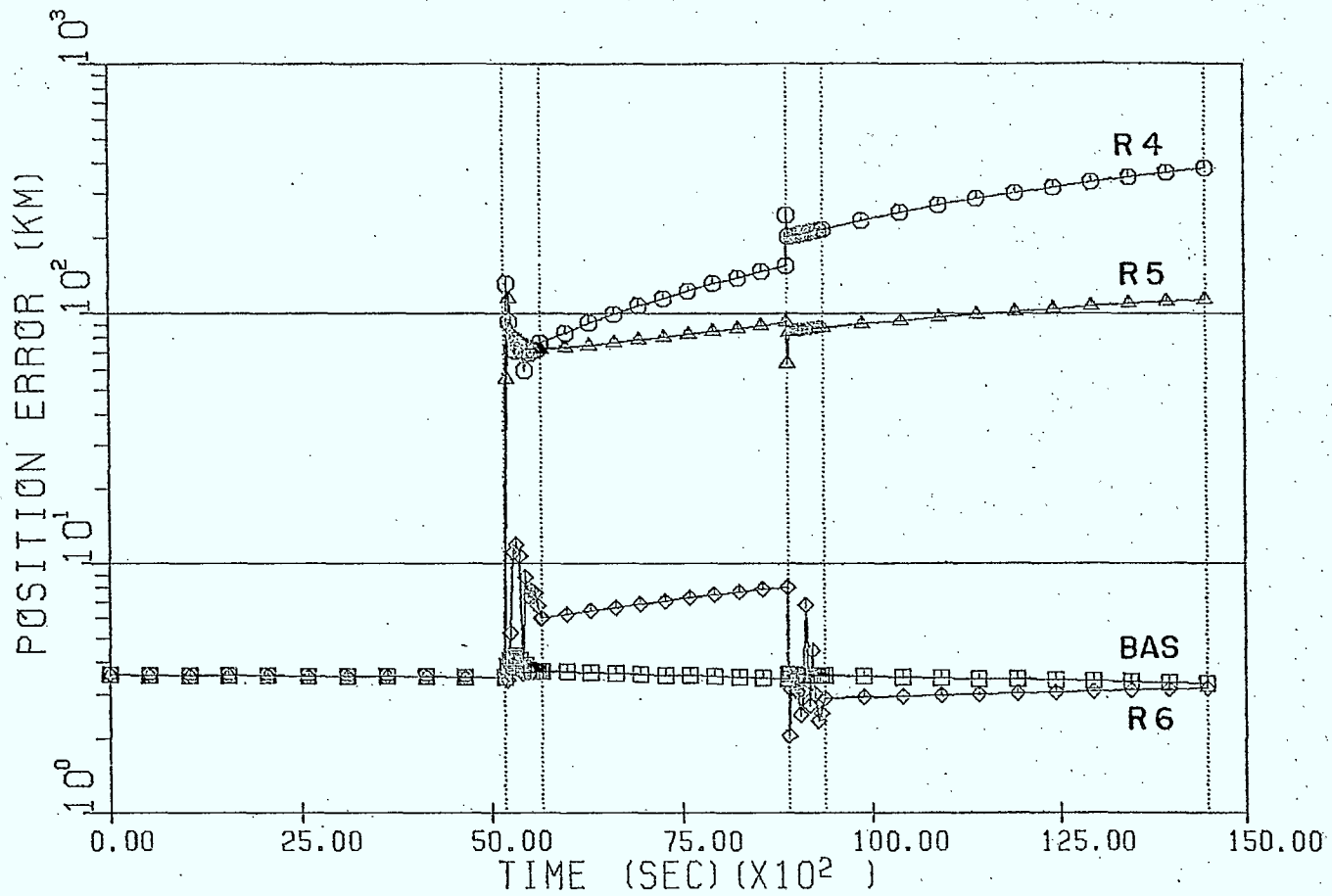
41

FIGURE 9. TYPICAL PERFORMANCE WHEN σ_ρ IS BELOW THE BASELINE
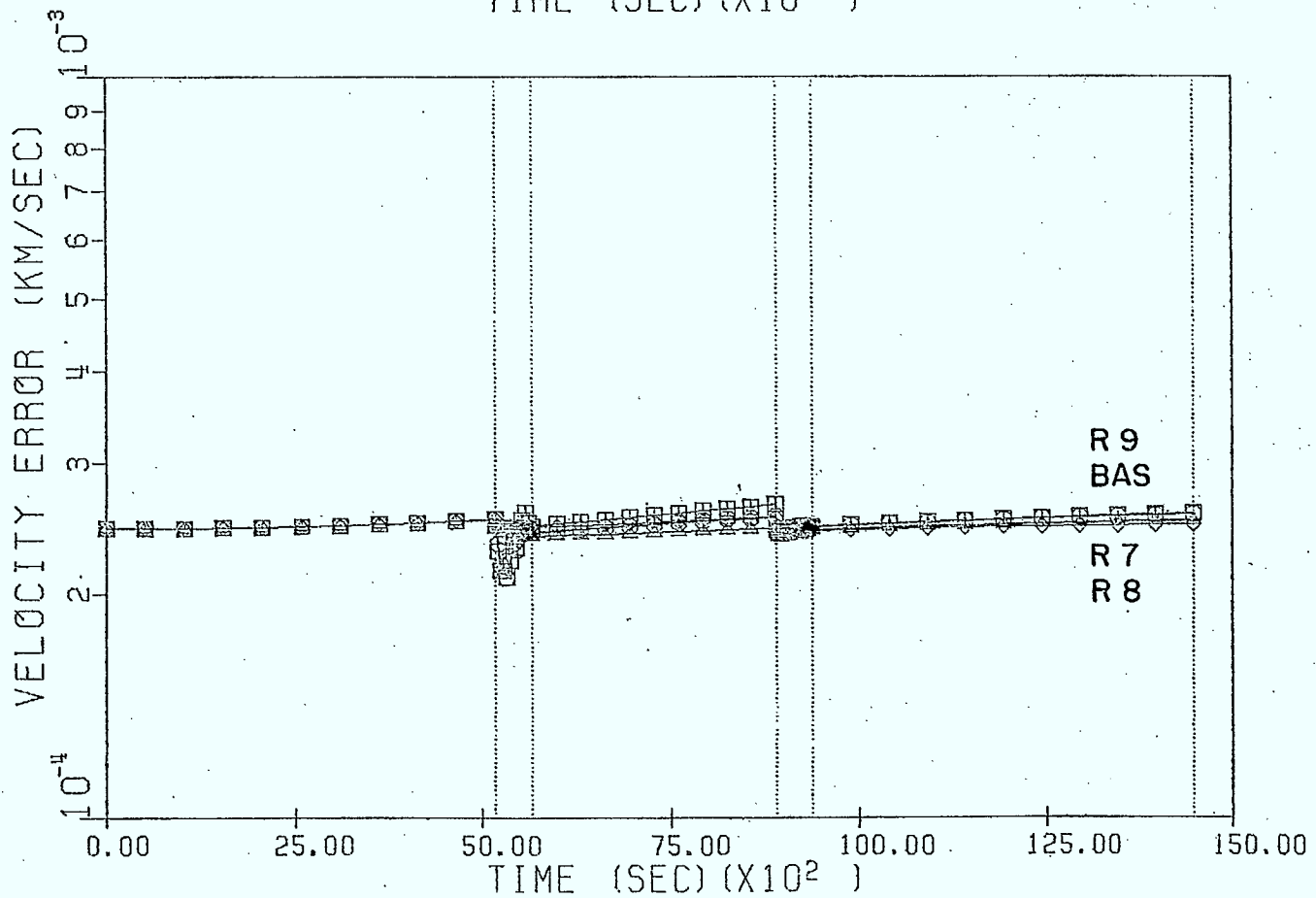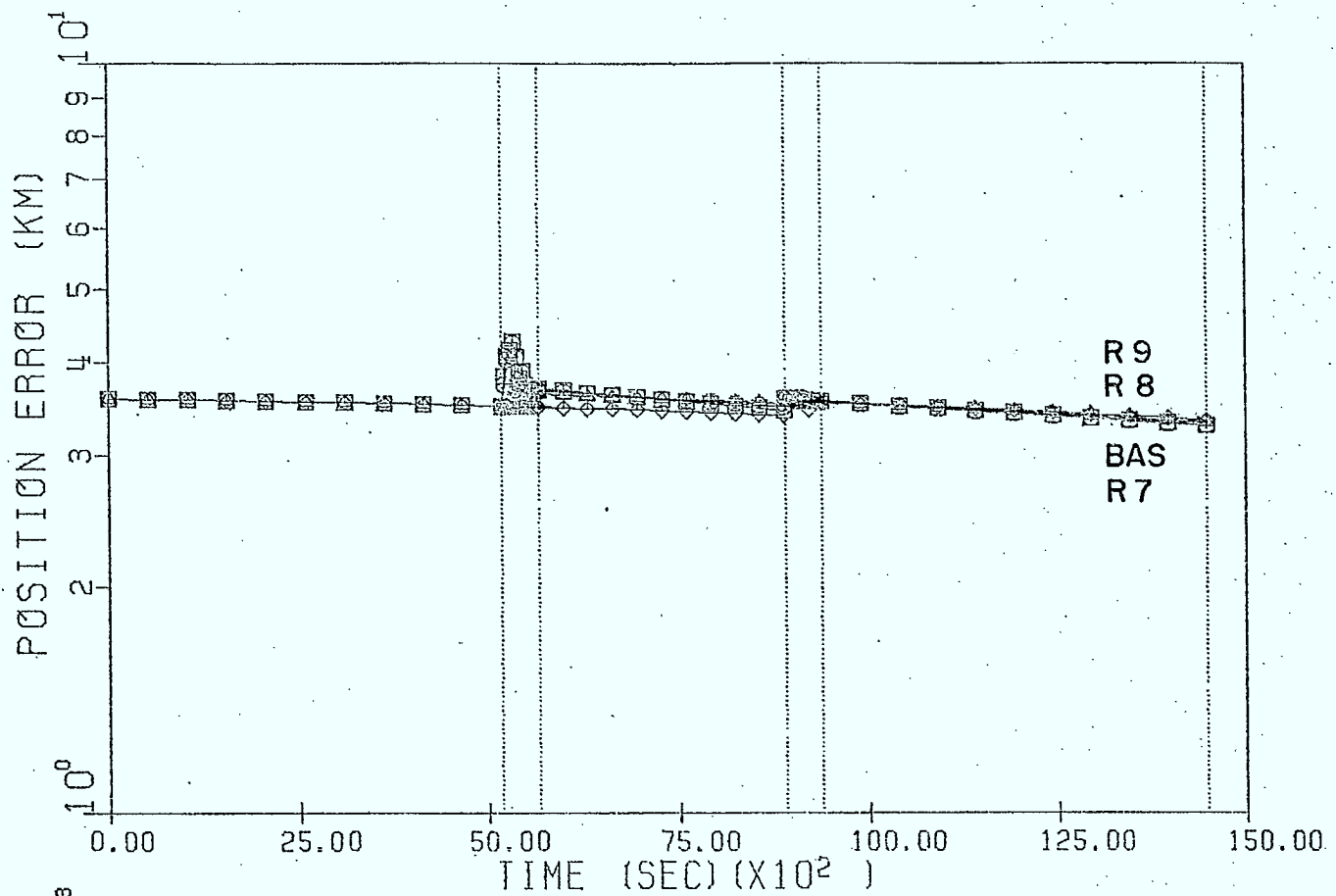VALUE.

FIGURE 10. TYPICAL PERFORMANCE WHEN σ_ρ IS ABOVE THE BASELINE
VALUE.

43

state noise study suggest, however, that a slightly better choice for σ_a might be a value between 10^{-8} and 10^{-7} km/sec^2 (corresponding to runs Q9 and Q10). Above these values the filter diverges (Fig. 11); below these values the filter performance is essentially the same as for the baseline σ_{aB} value (Fig. 12). In fact, for Q1 through Q7, regardless of whether or not P is diagonalized after the first observation, the final position and velocity errors are the same, to four significant digits, as those obtained using the baseline value of σ_a. In the divergent cases a nondiagonalized P matrix produces better results.

Even after recognizing that the baseline value chosen for σ_a is not optimal, the improvement that can be expected in the filter performance by readjusting σ_a is not staggering, as witnessed to by Figs. 11 and 12. Again, one would not expect to achieve the performance shown in Figs. 3 and 4 for an ideal geostationary orbit. At this juncture it should be mentioned that prior to adopting the form for the state noise matrix given in Appendix B a number of trial and error runs were conducted assuming a diagonal Q matrix. For some of these runs the values along the diagonal fell within the range suggested by $\sigma_a = [10^{-8}, 10^{-7}]$. Typically, the filter diverged (the remaining parameters were within the tolerances suggested by the above parameter studies). It would appear that the choice of the form for the state noise matrix is important, at least for geostationary orbits.

Given that the form for the state noise matrix derived in Appendix B is for a reference orbit that is exactly geostationary, whereas in ODPAC the reference orbit is based on the current best estimate of the state, two approaches suggest themselves for future work. One is to fix the
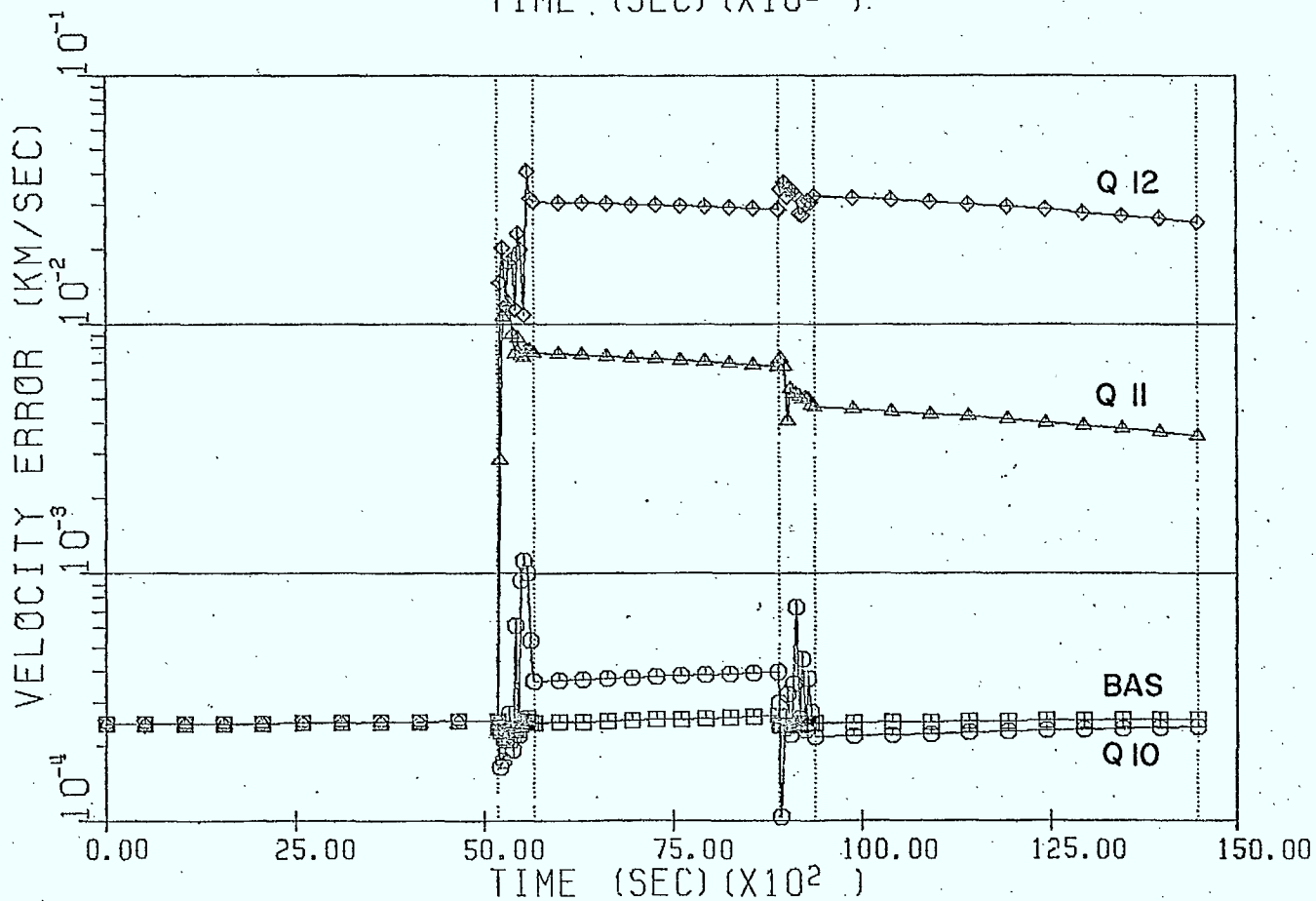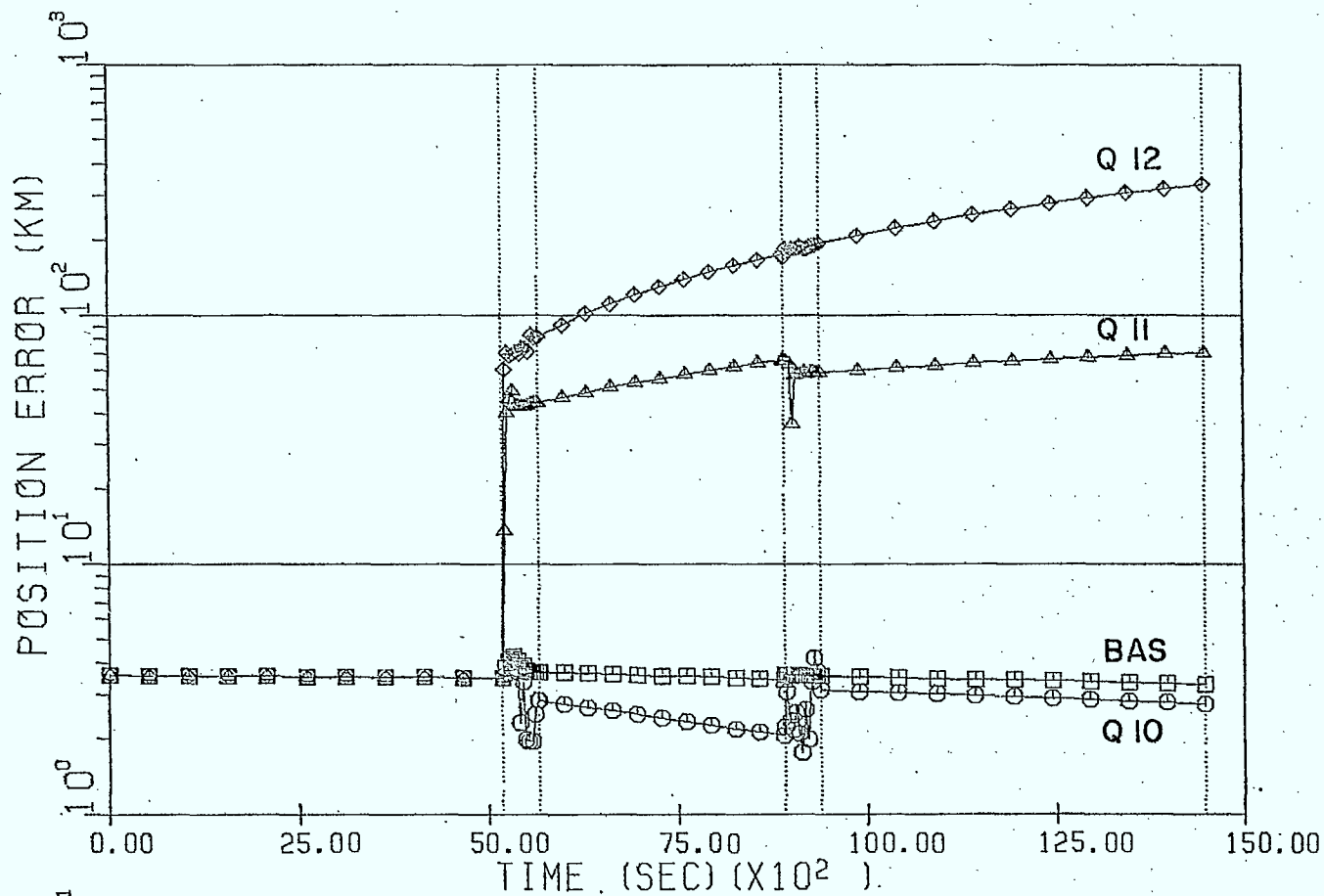
44

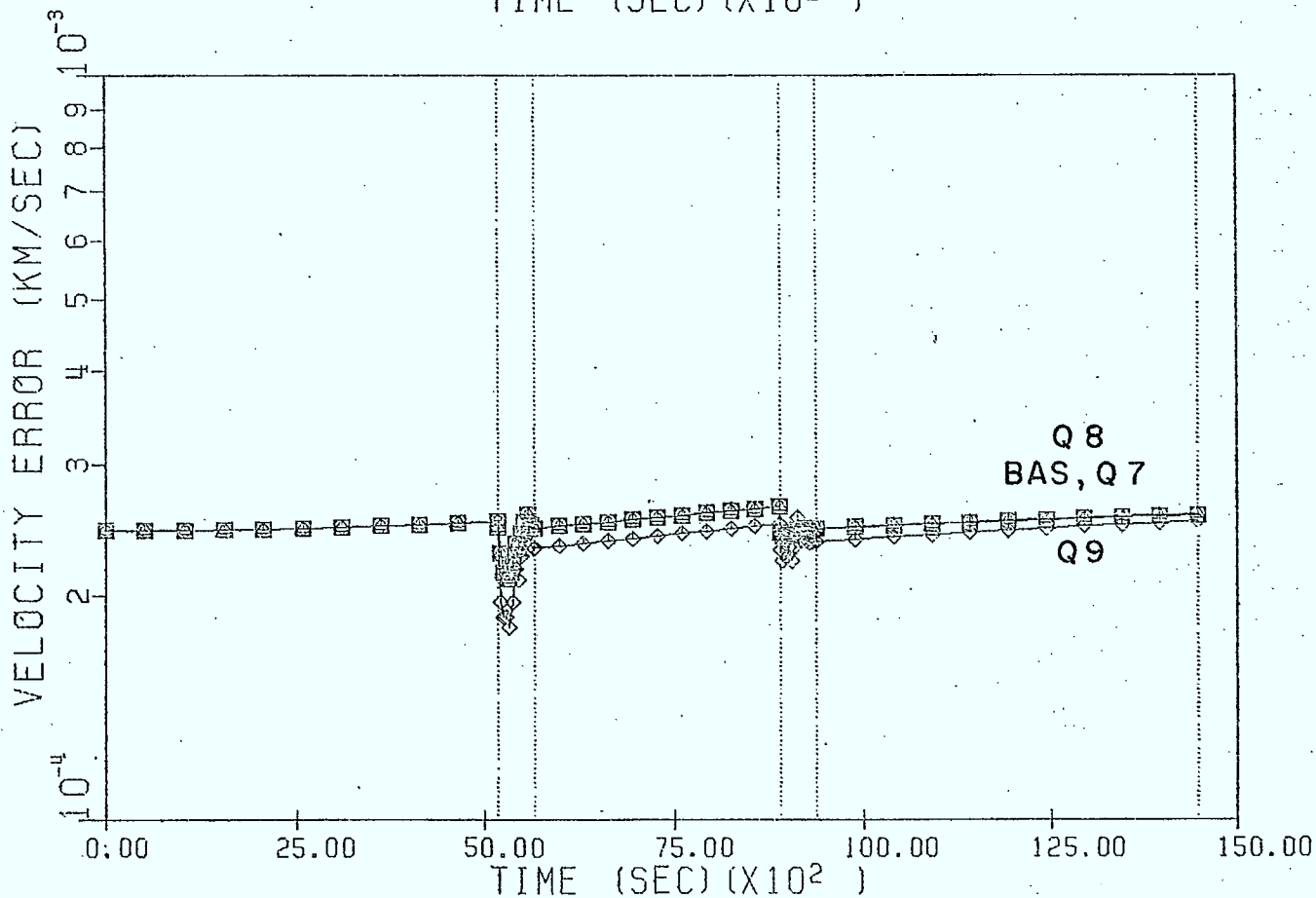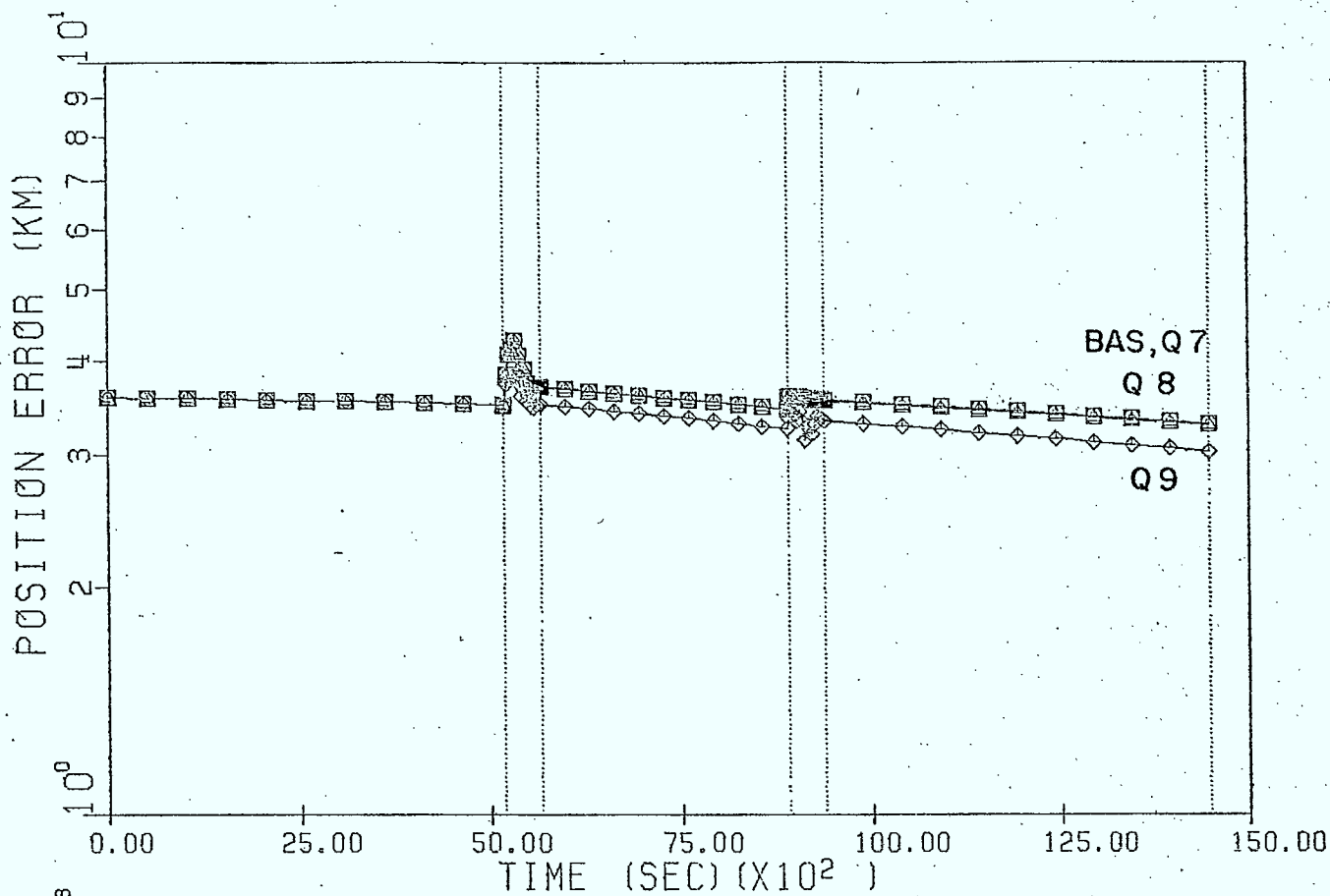FIGURE 11. TYPICAL PERFORMANCE WHEN σ_a IS ABOVE 10^{-7} KM/SEC.

45

FIGURE 12.   TYPICAL PERFORMANCE WHEN σ_a IS BELOW 10^{-8} KM/SEC.

46

reference orbit to be geostationary in ODPAC when estimating an orbit that is approximately geostationary. This would also have the effect of fixing the form of the state transition matrix Φ (see Appendix A). The other is to attempt to derive an analytical expression for Q based on a reference orbit that is only approximately geostationary. Figures 3 and 4 suggest this may be a reasonable approach.

Finally, as described in Appendix B, the chosen form for Q includes only the state noise resulting from the practice of neglecting perturbing accelerations when the state transition matrix is formulated. It may be possible to improve performance by retaining the present form for Q, and arbitrarily introducing extra terms along the diagonal to model random noise. This method may not appear to hold much promise given the problems encountered with a purely diagonal Q; however, the off-diagonal Q-terms may counter this effect. It should also be mentioned that GTDS does, in fact, include the partial derivatives of the perturbing accelerations relative to the state in the variational equations. This is equivalent to retaining the perturbing accelerations when computing the state transition matrix. While normally this does not appear to cause a problem, we note that here, when a conscious effort is made to re-introduce these unmodeled accelerations through Q, the Kalman filter performance can be made to be neutrally stable rather than divergent. It is possible that some property of a geostationary orbit makes significant the perturbative accelerations when finding the state transition matrix. For the present, this is speculation until supported by factual results.

6. CONCLUDING REMARKS

An attempt has been made to ascertain the contributing factors in the relatively poor performance of the ODPAC Kalman Estimator vis-a-vis the GTDS Least-Squares Estimator. It can be argued that the perturbation models used in both programs are essentially the same, however, a noticeable difference still results in the simulated true-state trajectories. This could be caused by the small differences in the perturbation models, but more likely it is a property of the type and order of the numerical integrator used in each case.

The Kalman estimator has been shown to perform well, using a state noise matrix based on a geostationary reference orbit, when the true-state trajectory is, indeed, geostationary. For an approximately geostationary orbit the filter performance degrades to the point of neutral stability. In this regard it performs poorly in comparison to GTDS. Furthermore, for the chosen initial error covariance, measurement noise and state noise matrices an extensive parameter study has shown that the filter performance cannot be improved substantially, in the present application, by simply changing the numerical values within these matrices. It appears that it may be useful to explore the possibility of deriving an alternate analytical form for the state noise matrix based on the assumption of an approximate, rather than an exact, geostationary orbit.

7. REFERENCES

1. Brogan, W. L., Lemay, J. L., "Autonomous Orbit Determination at Synchronous Altitude," AAS Paper No. 68-129, AAS/AIAA Astrodynamics Specialist Conference, Jackson, Wyoming, September 3-5, 1978.

2. Brogan, W. L., Lemay, J. L., "Autonomous Satellite Navigation--An Historical Summary and Current Status," Paper No. 21-1, Proceedings 1973 JACC Conference, June, 1973.

3. Browne, H. J., McPherson, E. A., "Orbit Determination and Prediction Mathematics," SED Document No. 91800-TR-101, Issue 3, SED System Inc., Saskatoon, Sask. (originally issued) August, 1978.

4. Browne, H. J., McPherson, E. A., "Orbit Determination Study: January 1978 Design Review," SED Document No. 083100-TR-101, Issue 1, SED System Inc., Saskatoon, Sask., January, 1978.

5. Cappellari, J. O., Velez, C. E., Fuchs, A. J., "Mathematical Theory of the Goddard Trajectory Determination System," Goddard Space Flight Center, NASA-TM-X-71106, April, 1976.

6. Chodas, P. W., "Application of the Extended Kalman Filter to Several Formulations of Orbit Determination," UTIAS Technical Note No. 224, August, 1981.

7. McPherson, E. A., Copeck, J. A., "Orbit Determination Prediction, and Correction (ODPAC) User's Manual," SED Document No. 381900-UM-101, Issue 1, SED System Inc., Saskatoon, Sask., October, 1980.

8. Soop, M., "Geostationary-Orbit Determination by Single-Ground-Station Tracking," European Space Agency (ESA) Journal, Vol. 4, 1980, pp. 158-169.

9. Steffan, K. F., "Orbital Guidance," Chapter 9 in Guidance and Control of Aerospace Vehicles, edited by C. T. Leondes, McGraw Hill, 1963.

10. Wakker, K. F., Ambrosius, B. A. C., "Kalman Filter Satellite Orbit Improvement Using Laser Ranging Measurements from a Single Tracking Station," AGARD-AG-No. 256; Advances in the Techniques and Technology of the Application of Nonlinear Filters and Kalman Filters, edited by C. T. Leondes, March, 1982, pp. 7-1, 7-16.

APPENDIX A

A CLOSED-FORM TRANSITION MATRIX

FOR A SATELLITE NOMINALLY IN GEOSTATIONARY ORBIT

In theory, if a satellite is placed in circular orbit (constant radius R) in the equatorial plane such that the angular velocity is directed along the orbit normal with magnitude $\omega = (\mu/R^3)^{\frac{1}{2}}$, where μ is the gravitational parameter for the Earth and $\omega/2\pi$ is the rotational period of the Earth ($\sim$ 24 sid. hr.), then the satellite remains stationary relative to the Earth, in what is denoted a geostationary orbit. In practice, environmental forces cause orbital perturbations, thus no satellite is truly geostationary. However, these perturbations are usually small enough so that the actual position vector to the spacecraft $\vec{r}$ can be written as the sum of a reference position vector $\vec{R}$ and a first-order (compared to $\vec{R}$) change in position $\vec{\varrho}$:

$$\vec{r} = \vec{R} + \vec{\varrho} \tag{A.1}$$

As shown in Fig. A-1, $\vec{R}$ (the radius vector of the geostationary reference orbit) is aligned with the x-axis of an orbiting frame F_O, while $\vec{\varrho}$ locates the spacecraft relative to $\vec{R}$. Here, the angular velocity of F_O with respect to an inertial frame F_I is denoted $\vec{\omega}$ and has the components

$$\underline{\omega} = [0,\ 0,\ \omega]^T \tag{A.2}$$

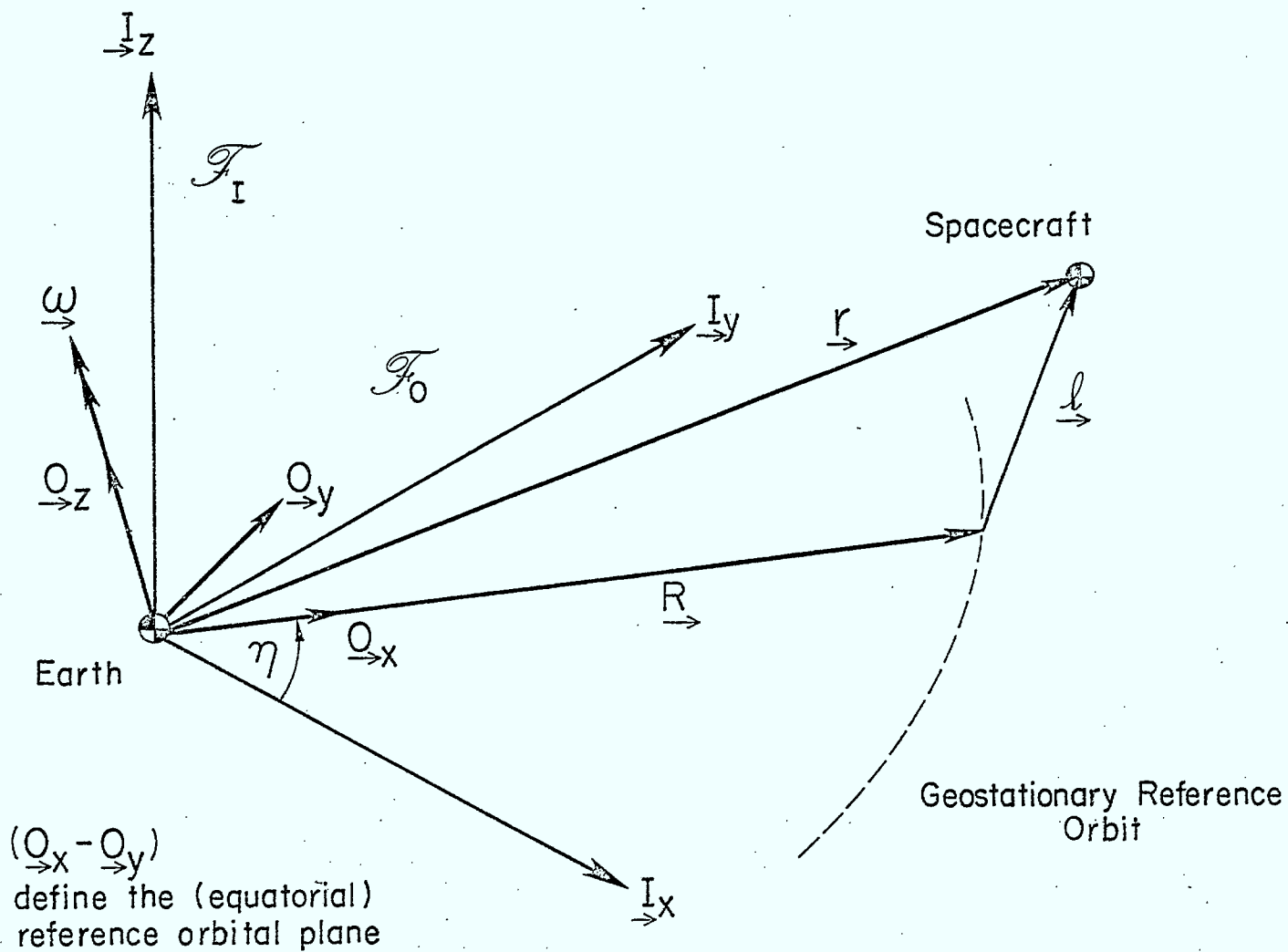expressed in F_O. As a consequence, F_O is related to F_I by the rotation matrix

FIGURE A-1. INERTIAL AND ORBITAL REFERENCE FRAMES.

$$C_{IO} = \begin{bmatrix} \cos\eta & -\sin\eta & 0 \\ \sin\eta & \cos\eta & 0 \\ 0 & 0 & 1 \end{bmatrix} \tag{A.3}$$

where η, the orbital anomaly of the geostationary reference orbit, obeys the relation

$$\dot{\eta} = \omega \tag{A.4}$$

Now the orbital equation of motion for the spacecraft is

$$\ddot{\vec{r}} + \frac{\mu}{r^3} \vec{r} = 0 \tag{A.5}$$

where

$$\vec{v} = \overset{\circ}{\vec{r}} + \vec{\omega} \times \vec{r} \tag{A.6}$$

$$\ddot{\vec{r}} = \overset{\circ}{\vec{v}} + \vec{\omega} \times \vec{v} \tag{A.7}$$

and perturbing accelerations have been neglected [d( )/dt with respect to F_I is denoted ($\dot{}$), while d( )/dt with respect to F_O is denoted ($\overset{\circ}{}$)]. This assumption echoes that made in determining the transition matrix assumed in ODPAC [Chodas, 1981]. Essentially, to update the estimate of the state a nonlinear state function including orbital perturbations is used, while to update the error covariance matrix a state transition matrix obtained neglecting orbital perturbations is applied.

Equation (A.5) can be expanded by noting (A.1), given the components of $\vec{R}$ and $\vec{\varrho}$, expressed in F_O, are

$$\underline{R} = [R, 0, 0]^T \tag{A.8}$$

$$\underline{\ell} = [x, y, z]^T \tag{A.9}$$

53

The result to first order in (ℓ/R), expressed in F_o, is [Steffan, 1963]

$$\begin{bmatrix} \ddot{x} - 2\omega\dot{y} - 3\omega^2 x \\ \ddot{y} + 2\omega\dot{x} \\ \ddot{z} + \omega z \end{bmatrix} = \begin{bmatrix} 0 \\ 0 \\ 0 \end{bmatrix} \tag{A.10}$$

The approximation

$$\frac{\vec{r}}{r^3} \cong \frac{1}{R^3}\left[(\vec{R} + \vec{\ell}) - 3\left(\frac{\vec{\ell}\cdot\vec{R}}{R^2}\right)\vec{R}\right] \tag{A.11}$$

based on the assumption

$$\ell \ll R \tag{A.12}$$

is also required to obtain (A.10). Integration of (A.10) yields

$$\begin{bmatrix} x \\ y \\ z \\ \dot{x} \\ \dot{y} \\ \dot{z} \end{bmatrix} \begin{bmatrix} (4x_o + 2\dot{y}_o/\omega) - (3x_o + 2\dot{y}_o/\omega)\cos\omega t + (\dot{x}_o/\omega)\sin\omega t \\ (y_o - 2\dot{x}_o/\omega) + 2(\dot{x}_o/\omega)\cos\omega t + (6x_o + 4\dot{y}_o/\omega)\sin\omega t - (6x_o + 3\dot{y}_o/\omega)\omega t \\ z_o\cos\omega t + (\dot{z}_o/\omega)\sin\omega t \\ (3\omega x_o + 2\dot{y}_o)\sin\omega t + \dot{x}_o\cos\omega t \\ -(6\omega x_o + 3\dot{y}_o) - 2\dot{x}_o\sin\omega t + (6\omega x_o + 4\dot{y}_o)\cos\omega t \\ \dot{z}_o\cos\omega t - \omega z_o\sin\omega t \end{bmatrix}$$

$$\tag{A.13}$$

where $[x_o, y_o, z_o, \dot{x}_o, \dot{y}_o, \dot{z}_o]^T$ is the initial state $(t = t_o)$. Equation (A.13) gives the orbital state relative to a geostationary reference orbit from t_o to t. As a consequence, the state transition matrix from time t_k to t_{k+1} ($\Delta t = t_{k+1} - t_k$) is, simply,

54

$$\phi(k+1,\ k) = \begin{bmatrix} \Phi_{rr}(k+1,\ k) & \Phi_{rv}(k+1,\ k) \\ \Phi_{vr}(k+1,\ k) & \Phi_{vv}(k+1,\ k) \end{bmatrix} \quad (A.14)$$

where

$$\phi_{rr}(k+1,\ k) = \begin{bmatrix} 4-3\cos\omega\Delta t & 0 & 0 \\ 6(\sin\omega\Delta t-\omega\Delta t) & 1 & 0 \\ 0 & 0 & \cos\omega\Delta t \end{bmatrix} \quad (A.15)$$

$$\phi_{rv}(k+1,\ k) = \begin{bmatrix} (1/\omega)\sin\omega\Delta t & (2/\omega)(1-\cos\omega\Delta t) & 0 \\ (2/\omega)(\cos\omega\Delta t-1) & (4/\omega)(\sin\omega\Delta t-3\Delta t) & 0 \\ 0 & 0 & (1/\omega)\sin\omega t \end{bmatrix} \quad (A.16)$$

$$\phi_{vr}(k+1,\ k) = \begin{bmatrix} 3\omega\sin\omega\Delta t & 0 & 0 \\ 6\omega(\cos\omega\Delta t-1) & 0 & 0 \\ 0 & 0 & -\omega\sin\omega\Delta t \end{bmatrix} \quad (A.17)$$

$$\phi_{vv}(k+1,\ k) = \begin{bmatrix} \cos\omega\Delta t & 2\sin\omega\Delta t & 0 \\ -2\sin\omega\Delta t & -3+4\cos\omega\Delta t & 0 \\ 0 & 0 & \cos\omega\Delta t \end{bmatrix} \quad (A.18)$$

In the present study the state is expressed in inertial rather than orbital coordinates, hence (A.14) must be transformed from F_O to F_I using (A.3). The desired state transition matrix is, therefore,

$$\Phi(k+1,\ k) = \begin{bmatrix} C_{IO}\phi_{rr}C_{OI} & C_{IO}\phi_{rv}C_{OI} \\ C_{IO}\phi_{vr}C_{OI} & C_{IO}\phi_{vv}C_{OI} \end{bmatrix} \quad (A.19)$$

55

where

$$C_{OI} = C_{IO}^{T} \qquad \qquad (A.20)$$

For the sake of brevity (A.19) is not written out in full; however, it is interesting to note that, for $(i = 1, 2, 4, 5; j = 3, 6)$ and for $(i = 3, 6; j = 1, 2, 4, 5)$, $\Phi_{ij} \equiv 0$.

APPENDIX B

A STATE NOISE MATRIX

FOR A SATELLITE NOMINALLY IN GEOSTATIONARY ORBIT

In formulating the state noise matrix used in ODPAC [Chodas, 1981], it is assumed that the linearized state obeys the equation

$$\delta \underline{x}_{k+1} = \Phi(t_{k+1}, t_k) \delta \underline{x}_k + \underline{w}_{k+1} \tag{B.1}$$

where $\delta \underline{x}_k$ is the state at time t_k, Φ is the state transition matrix and $\underline{w}_k$ is a sequence of random vectors called the state noise. It is assumed that the state noise behaves as white Gaussian noise and obeys the following relations for all k and j:

$$E\{\underline{w}_k\} = 0 \tag{B.2}$$

$$E\{\underline{w}_k \ \underline{w}_j^T\} = Q_k \ \underline{\delta}_{kj} \tag{B.3}$$

where E{ } denotes expectation, Q_k is the state noise matrix at time t_k and δ_{kj} is the Kronecker delta. Unfortunately, one source of state noise, namely, the perturbative environmental accelerations neglected in deriving Φ (see [Chodas, 1981] and Appendix A) are not random, nor, in general, will their expected values be zero, as assumed in (B.2). As a consequence, one should define a modified state noise matrix

$$Q_k = Q_k^n + Q_k^u \tag{B.4}$$

where Q_k^n is the state noise matrix in the sense of (B.2) and (B.3) and Q_k^u is the state 'noise' from unmodeled accelerations.

[Brogan and Lemay, 1968] derive an expression for Q_k^u, when the reference orbit about which the state function $f(x, \zeta, t)$ is linearized, is geostationary. Paraphrasing, let $\underline{\zeta}$ represent all of the parameters affecting the original state function and let $\delta\underline{\zeta}$ be the deviation of $\underline{\zeta}$ from the parameters affecting the reference geostationary orbit (in the same sense as $\delta\underline{x}$ is related to $\underline{x}$). Then, the linearized state equation becomes

$$\dot{\delta\underline{x}} = F(t)\delta\underline{x} + Z(t)\delta\underline{\zeta} \qquad (B.5)$$

where

$$F(t) = \frac{\partial f}{\partial x^T} (\bar{\underline{x}}, \bar{\underline{\zeta}}, t) \qquad (B.6)$$

$$Z(t) = \frac{\partial f}{\partial \zeta^T} (\bar{\underline{x}}, \bar{\underline{\zeta}}, t) \qquad (B.7)$$

and $(\bar{\underline{x}}, \bar{\underline{\zeta}})$ are the reference values for $(\underline{x}, \underline{\zeta})$. The solution to (B.5), assuming time is discretized, is

$$\delta\underline{x}_{k+1} = \Phi(t_{k+1}, t_k)\delta\underline{x}_k + q_{k+1} \qquad (B.8)$$

where

$$\underline{q}_{k+1} = \int_{t_k}^{t_{k+1}} \Phi(t_{k+1}, \tau)Z(\tau)\delta\underline{\zeta}(\tau)d\tau \qquad (B.9)$$

In reality, all the $\underline{\zeta}$ may not be identifiable and there may even be $\delta\underline{\zeta}$ components of which the analyst is unaware (the unknown unknowns). In the first case, the best one can hope for, if all the perceived $\delta\underline{\zeta}$ cannot be identified or modeled, is that their contribution $Z(t)\delta\underline{\zeta}(t)$ to the linearized state equation can at least be determined. In the second case, the best one can do is assume a noise term such as $\underline{w}_{k+1}$ in equation (B.1) to compensate for totally unknown quantities.

58

For the present situation, assuming the only parameters not grouped in a term such as $\underline{w}_{k+1}$ are those which produce the perturbative unmodeled accelerations $\delta\underline{a}(t)$, then

$$Z(t)\delta\underline{\zeta}(t) = [0, \ 0, \ 0, \ C_{IO} \ \delta\underline{a}(t)]^T \tag{B.10}$$

where the components of $\delta\underline{a}(t)$ are expressed in the orbital frame F_O, defined in Appendix A. Hence, the introduction of the rotation matrix C_{IO} which relates the frame F_O to inertial space F_I [(A.3) of Appendix A]. Presently, (B.9) is assumed to be written in inertial coordinates. This is necessary because, of the various coordinate systems available within ODPAC, an inertial one provides the most convenient mode for comparison with GTDS run results. (The chosen GTDS case integrates in inertial coordinates.) Also, the orbital coordinate system F_O, chosen for analytical reasons in Appendix A, is not available within ODPAC. Unfortunately, the integrand of (B.9) is most easily evaluated for Φ expressed in F_O. The most useful form [given (A.19)] is, therefore,

$$\underline{q}_{k+1} = \int_{t_k}^{t_{k+1}} \begin{bmatrix} C_{IO}\phi_{rr}(t_{k+1}, \ \tau)C_{OI} & C_{IO}\phi_{rv}(t_{k+1}, \ \tau)C_{OI} \\ C_{IO}\phi_{vr}(t_{k+1}, \ \tau)C_{OI} & C_{IO}\phi_{vv}(t_{k+1}, \ \tau)C_{OI} \end{bmatrix} \begin{bmatrix} 0 \\ C_{IO} \ \delta\underline{a}(\tau) \end{bmatrix} d\tau$$

$$= \int_{t_k}^{t_{k+1}} \begin{bmatrix} C_{IO}\phi_{rv}(t_{k+1}, \ \tau)\delta\underline{a}(\tau) \\ C_{IO}\phi_{vv}(t_{k+1}, \ \tau)\delta\underline{a}(\tau) \end{bmatrix} d\tau \tag{B.11}$$

Now, for state update intervals $\Delta t = (t_{k+1} - t_k)$ which are small compared to the 24-hour period of the reference geostationary orbit, $\delta\underline{a}(t)$ can be approximated by a constant average value $\delta\underline{a}$ over each Δt. Furthermore, it is reasonable to assume η to be quasi-static for small Δt, so that

setting η equal to its average value over the interval enables C_{IO} to be taken outside the integral in (B.11). Finally, for small Δt, ϕ_{rv} (A.16) and ϕ_{vv} (B.18) can be approximated by retaining only terms linear in Δt. Given these three approximations, (B.11) becomes

$$
\underline{q}_{k+1} = \begin{bmatrix} C_{IO} & 0 \\ 0 & C_{IO} \end{bmatrix} \begin{bmatrix} \delta a_x \Delta t^2/2 \\ \delta a_y \Delta t^2/2 \\ \delta a_z \Delta t^2/2 \\ \delta a_x \Delta t + \omega \delta a_y \Delta t^2 \\ \delta a_y \Delta t - \omega \delta a_x \Delta t^2 \\ \delta a_z \Delta t \end{bmatrix}
\tag{B.12}
$$

The matrix Q_{k+1}^u is then found by forming

$$
E\{\underline{q}_{k+1} \; \underline{q}_j^T\} = Q_{k+1}^u \; \delta_{k+1j}
\tag{B.13}
$$

where (B.2) no longer applies in general. Now, assuming $E\{\delta a_x^2\} = E\{\delta a_y^2\} = E\{\delta a_z^2\} = \sigma_a^2$ and that $E\{\delta a_x \; \delta a_y\} = E\{\delta a_x \; \delta a_z\} = E\{\delta a_x \; \delta a_z\} = 0$, substituting (B.12) into (B.13) yields

$$
Q_{k+1}^u = \sigma_a^2 \begin{bmatrix} Q_{rr} & Q_{rv} \\ Q_{vr} & Q_{vv} \end{bmatrix}
\tag{B.14}
$$

where

$$
Q_{rr} = \begin{bmatrix} \Delta t^4/4 & 0 & 0 \\ 0 & \Delta t^4/4 & 0 \\ 0 & 0 & \Delta t^4/4 \end{bmatrix}
\tag{B.15}
$$

60

$$Q_{rv} = \begin{bmatrix} \Delta t^3/2 & -\omega\Delta t^4/2 & 0 \\ \omega\Delta t^4/2 & \Delta t^3/2 & 0 \\ 0 & 0 & \Delta t^3/2 \end{bmatrix} = Q_{vr}^T \qquad (B.16)$$

$$Q_{vv} = \begin{bmatrix} \Delta t^2(1+\omega^2\Delta t^2) & 0 & 0 \\ 0 & \Delta t^2(1+\omega^2\Delta t^2) & 0 \\ 0 & 0 & \Delta t^2 \end{bmatrix} \qquad (B.17)$$

One last observation must be made before (B.14) can be used as a state 'noise' model in ODPAC, where the state noise matrix is assumed proportional to Δt. That is, ODPAC evaluates

$$Q = Q'\Delta t \qquad (B.18)$$

where Q' is stored in SNC. Hence, to use (B.14) in ODPAC, Q_{k+1}^u must be divided by Δt prior to being stored in SNC.

APPENDIX C

SOME COMMENTS ON ODPAC

In this appendix, some point-form comments on the problems, limitations and advantages of ODPAC [McPherson and Copeck, 1980] are summarized.

- The ODPAC simulator-file storage system was found to be limited.

- It would be useful to have the capability of inputting the true state trajectory from an external disk file or tape.

- The available integration schemes are limited.

- The interactive feature is very helpful in learning the system and for runs of reasonably short duration; however, for long runs the batch facility was found very useful.

- The commands are well designed, easily learned, and easy to use.

- The user's manual deserves equal praise.

- The inability to change or enter only selected elements in the true and estimated state vectors, and in the error covariance and state noise matrices, is a large inconvenience.

SINCARSIN, G.B.
   Geostationary orbital estimation
using a kalman filter

DATE DUE
DATE DE RETOUR

MAY 3 1 1985			

LOWE-MARTIN No. 1137